J. Fluid Mech. (2007), *vol.* 575, *pp.* 333–357. © 2007 Cambridge University Press
doi:10.1017/S0022112006004046 Printed in the United Kingdom

Particle motion near and inside an interface

C. POZRIKIDIS

Department of Mechanical and Aerospace Engineering, University of California, San Diego, La Jolla, CA 92093-0411, USA

(Received 15 July 2006 and in revised form 22 September 2006)

The motion of a spherical particle near the interface between two immiscible viscous fluids undergoing simple shear flow is considered in the limit of small Reynolds and capillary numbers where the interface exhibits negligible deformation. Taking advantage of the rotational symmetry of the boundaries of the flow with respect to the axis that is normal to the interface and passes through the particle centre, the problem is formulated as a system of one-dimensional integral equations for the first Fourier coefficients of the unknown components of the traction and velocity along the particle and interface contours. The results document the particle translational and angular velocities, and reveal that the particle slips while rolling over the interface under the influence of a simple shear flow, for any viscosity ratio. In the second part of the investigation, the motion of an axisymmetric particle straddling a planar interface is considered. The results confirm a simple exact solution when a particle with top-down symmetry is immersed half-way in each fluid and translates parallel to the interface, reveal a similar simple solution for a particle that is held stationary in simple shear flow, and document the force and torque exerted on a spherical particle for more general arrangements. The onset of a non-integrable singularity of the traction at the contact line prohibits the computation of the translational and angular velocities of a freely suspended particle convected under the action of a shear flow.

1. Introduction

Efforts to describe the motion and assess the significance of small particles, liquid drops, and gas bubbles in two-phase and interfacial flow have led to studies of particle motion near interfaces between two immiscible fluids. In some cases, the fluids are quiescent and the flow is induced by the particle motion alone. In other cases, heavy, buoyant, or freely suspended particles are convected in a specified flow. In most cases, the motion occurs under conditions of Stokes flow due to the small particle size. In the pioneering work of Aderogba (1976) and Aderogba & Blake (1978*a*, *b*), the flow induced by a point force near a flat interface was computed in terms of singular solutions of the equations of Stokes flow, and the particle-induced deformation of the interface was displayed. This fundamental solution constitutes a building block for describing the motion of distant particles using the method of reflections.

The majority of theoretical studies have addressed the flow induced by particle motion in an otherwise quiescent environment. O'Neill & Ranger (1979), Lee, Chadwick & Leal (1979), Lee & Leal (1980, 1982), and Berdan & Leal (1982) studied the flow due to the translation and rotation of a sphere. Yang & Leal (1983) and Fulford & Blake (1983) considered the motion of a slender particle resembling a rod, and Yang & Leal (1989) studied the motion of a porous particle. Falade (1986) generalized the asymptotic analysis to small particles with arbitrary shape and far-field

https://doi.org/10.1017/S0022112006004046 Published online by Cambridge University Press

flows. More recently, Danov *et al.* (1998) investigated the significance of interfacial rheology and found that surface viscosity becomes important at small separations.

Less attention has been paid to the motion of freely-suspended particles convected under the action of a shear, extensional, or more general flow. Yang & Leal (1983, 1984) considered the motion of spherical and slender particles by asymptotic expansions, and Stoos & Leal (1989) computed motions in axisymmetric elongational flow. In a series of papers, Leal and coworkers studied corresponding problems involving liquid drops (i.e. Yang & Leal 1990). Notable is the work of Yiantsios & Davis (1990), who performed a lubrication-flow analysis for the motion of a drop normal to an interface or plane wall. Configurations involving axisymmetric flows considerably simplify the analysis by permitting the use of streamfunctions and the application of effectively one-dimensional boundary integral representations.

A few authors considered the motion of particles straddling an interface in order to describe the micromechanics of interfacial species transport and predict the surface Brownian diffusivity in terms of the mobility using the Stokes–Einstein relationship. Ranger (1978) considered the normal and tangential motion of a thin circular disk straddling a planar interface between two immiscible liquids with arbitrary viscosities, and O'Neill, Ranger & Brenner (1986) and Stoos & Leal (1990) considered the motion of a spherical particle straddling a flat free surface. Danov, Dimova & Pouligny (2000) investigated the motion of a particle straddling a spherical interface and incorporated the effect of interfacial rheology. Their study was motivated by laboratory observations of microspheres attached to vesicles reported by Velikov *et al.* (1997). In a personal communication, Professor K. D. Danov pointed out that taking measurements of the trajectories of tracers over an interface is the only available means for assessing the rheology of structured interfaces and biological membranes. To interpret laboratory data accurately, the resistance to the motion due to the bulk-phase viscosity must be available.

When the boundary conditions specify a non-zero particle surface velocity normal to the contact line, a non-integrable singularity in the stress arises, yielding an infinite force. This strong singularity appears when a spherical particle rotates around an axis that is parallel to the interface or is freely convected in simple shear flow, but not when the particle translates parallel to the interface or is held stationary in a simple shear flow. To prevent the divergence of the hydrodynamic stress, O'Neill *et al.* (1986) replaced the no-slip boundary condition over the particle surface with the Navier slip boundary condition. This regularization is physically acceptable in light of the molecular size of the particles considered.

In § 2, we study the motion of a freely suspended spherical particle in simple shear flow parallel to an interface between two fluids with arbitrary viscosities in the limit of vanishing Reynolds number. The main objective is to compute the particle translational and angular velocities for arbitrary particle-to-interface separations in the limit of small capillary number where the interface deformation is small and can be neglected to a first approximation. The numerical results extend previous asymptotic solutions by Yang & Leal (1983, 1984) for large particle-to-interface separations and illustrate the flow kinematics and interfacial deformation to leading order with respect to the capillary number.

In § 3, we consider the motion of a spherical particle straddling a flat interface. A symmetry argument suggests that the flow due to the in-plane translation of an axisymmetric particle with up-to-down symmetry with respect to the interface can be constructed in terms of the flow in infinite space using corresponding fluid viscosities, in agreement with the results of Ranger (1978) and O'Neill *et al.* (1986).

https://doi.org/10.1017/S0022112006004046 Published online by Cambridge University Press

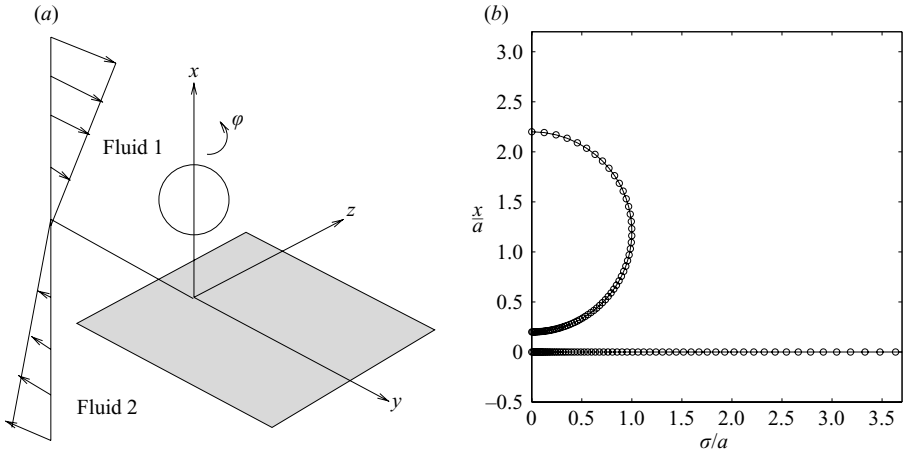


FIGURE 1. (*a*) Illustration of a spherical particle near a flat interface between two immiscible viscous fluids undergoing simple shear flow. (*b*) Typical discretization of the particle and interface contour in a meridional plane.

Examples of such shapes include the disk and the half-submerged sphere. A similar symmetry argument suggests that superposition is also possible when the particle is held stationary in an incident simple shear flow. Numerical results will be presented for the force and torque exerted on the particle for more general configurations.

Accurate computations for both problems will become feasible by exploiting the axial symmetry of the domain of flow to simplify the boundary integral representation of the genuinely three-dimensional flow. The reduction yields a system of one-dimensional integral equations for the first Fourier coefficients of the boundary traction and free-surface velocity defined over the various boundary contours in a meridional plane. The solution can be solved accurately and efficiently by elementary boundary element methods. Although a similar methodology has been used previously to compute flow past surfaces with axisymmetric irregularities in the form of a particle, a depression, or a protrusion and the motion of a particle in film flow (Pozrikidis 1994*a*, *b*, 1997*b*, 2000, 2006; Matzen 1997; Shatz 2004), the implementation for interfacial flow is a new adventure.

2. A spherical particle near an interface

We consider the steady motion of a spherical particle of radius a near the planar interface between two viscous fluids undergoing simple shear flow (figure 1). The upper fluid is designated by the index 1, and the lower fluid is designated by the index 2. The x-axis is perpendicular to the interface and passes through the particle centre, the y-axis points in the direction of the incident shear flow, and the z-axis is orthogonal to both. Far from the particle, the velocity field designated by the superscript ∞ is given by $u_x^\infty = 0$, $u_y^\infty = k_i x$, and $u_z^\infty = 0$, where k_i is the shear rate in the ith fluid. Continuity of shear stress at the interface requires $k_1 = \lambda k_2$, where $\lambda = \mu_2/\mu_1$ is the ratio of the fluid viscosities. We will assume that the particle is neutrally buoyant so that gravity does not drive it toward or away from the interface. The combined gravity- and shear-driven motion can be constructed by linear superposition.

The particle generates a disturbance flow, denoted by the superscript D, that may be added to the simple shear flow to yield the total flow with velocity $\boldsymbol{u} = \boldsymbol{u}^\infty + \boldsymbol{u}^D$ and

https://doi.org/10.1017/S0022112006004046 Published online by Cambridge University Press

pressure $p = p^{\infty} + p^{D}$. Near the particle, the simple shear flow and the disturbance flow have comparable magnitudes. The Reynolds number written with respect to the particle size is assumed to be sufficiently small that the motion of the fluid is governed by the equations of Stokes flow,

$$-\nabla p + \mu \nabla^2 \boldsymbol{u} + \rho \boldsymbol{g} = \boldsymbol{0}, \qquad \nabla \cdot \boldsymbol{u} = 0, \tag{2.1}$$

where ρ is the fluid density and $\boldsymbol{g}$ is the acceleration of gravity, assumed to be normal to the interface. The no-slip and no-penetration boundary conditions require $\boldsymbol{u} = \boldsymbol{V} + \boldsymbol{\Omega} \times (\boldsymbol{x} - \boldsymbol{x}_c)$ over the particle surface, where $\boldsymbol{V}$ is the velocity of translation of the particle centre, $\boldsymbol{x}_c = (x_c, 0, 0)$, and $\boldsymbol{\Omega}$ is the angular velocity of rotation about $\boldsymbol{x}_c$. Analogous boundary conditions require that the fluid velocity is continuous across the interface. In the absence of surfactants, the shear stress is continuous across the interface, $\boldsymbol{n} \times \Delta \boldsymbol{f} \times \boldsymbol{n} = \boldsymbol{0}$, where $\Delta q = q_1 - q_2$ denotes the interfacial jump of the variable q, $\boldsymbol{f} \equiv \boldsymbol{\sigma} \cdot \boldsymbol{n}$ is the traction, $\boldsymbol{\sigma}$ is the stress tensor in each fluid, and $\boldsymbol{n}$ is the unit normal vector pointing into the upper fluid labelled 1. The normal stress suffers a discontinuity determined by the surface tension, γ, given by $\Delta \boldsymbol{f} \cdot \boldsymbol{n} = 2\kappa_m \gamma \boldsymbol{n}$, where κ_m is the mean curvature computed from $2\kappa_m = \nabla_s \cdot \boldsymbol{n}$, $\nabla_s = (\boldsymbol{I} - \boldsymbol{nn}) \cdot \nabla$ is the tangential gradient, and $\boldsymbol{I}$ is the identity matrix.

We restrict our attention to situations where the surface tension is strong enough to prevent significant deformation of the interface from the undisturbed flat shape. The formal requirement is that the capillary number, $Ca = \mu_1 k_1 a / \gamma$, be sufficiently small. To derive appropriate boundary conditions, we describe the interface as $x = \eta(y, z) = a\, Ca\, \phi(y, z)$, where $\phi(y, z)$ is a dimensionless shape function, and expand the velocity, stress, and normal vector in perturbation series with respect to Ca,

$$\left.\begin{aligned} &\boldsymbol{u} = \boldsymbol{u}^{\infty} + \boldsymbol{u}^{D(0)} + Ca\, \boldsymbol{u}^{D(1)} + \cdots, \quad \boldsymbol{\sigma} = \boldsymbol{\sigma}^{\infty} + \boldsymbol{\sigma}^{D(0)} + Ca\, \boldsymbol{\sigma}^{D(1)} + \cdots, \\ &\boldsymbol{n} = \boldsymbol{e}_x + Ca\, \boldsymbol{n}^{(1)} + \cdots, \end{aligned}\right\} \tag{2.2}$$

where $\boldsymbol{e}_x$ is the unit vector along the x axis. Next, we shift the interface from the actual location to the undisturbed position and transfer the boundary conditions using the method of domain perturbation. When the particle translates parallel to the interface, the interfacial shape as seen by an observer travelling with the particle is stationary and the normal velocity component vanishes, $(\boldsymbol{u}(x = \eta) - \boldsymbol{V}) \cdot \boldsymbol{n} = 0$. Making substitutions, we find

$$\big(\boldsymbol{u}^{\infty}(x = 0) + \boldsymbol{u}^{D(0)}(x = 0) - \boldsymbol{V}\big) \cdot \boldsymbol{e}_x + O(Ca) = 0, \tag{2.3}$$

yielding $u_x^{D(0)} \sim O(Ca)$ for both fluids. Next, we consider the dynamic boundary condition $(\Delta \boldsymbol{\sigma}) \cdot \boldsymbol{n} = 2\kappa_m \gamma \boldsymbol{n}$, approximate the mean curvature with $2\kappa_m \simeq -\nabla^2 \eta$ (e.g. Pozrikidis 1997*a*), and work in a similar fashion to find

$$\big(\Delta \boldsymbol{\sigma}^{\infty}(x = 0) + \Delta \boldsymbol{\sigma}^{D(0)}(x = 0)\big) \cdot \boldsymbol{e}_x + O(Ca) = -\mu_1 k_1 a^2 \nabla^2 \phi \boldsymbol{e}_x + O(Ca), \tag{2.4}$$

where ∇^2 is the Laplacian with respect to y and z. Thus,

$$\Delta f_x^{D(0)} = -\mu_1 k_1 a^2 \nabla^2 \phi + O(Ca), \quad \Delta f_y^{D(0)} \sim O(Ca) \quad \Delta f_z^{D(0)} \sim O(Ca), \tag{2.5}$$

where $\Delta f_x^{D(0)} \equiv \Delta \boldsymbol{\sigma}^{D(0)}(x = 0) \cdot \boldsymbol{e}_x$. In summary, the x velocity component and the y and z traction components of the leading-order disturbance flow are zero over the flat interface. The kinematic condition of zero normal velocity replaces the usual dynamic condition requiring that the normal component of the traction jump be balanced by the capillary force due to the surface tension. In the remainder of the paper, the

https://doi.org/10.1017/S0022112006004046 Published online by Cambridge University Press

superscript (0) will be suppressed, and the disturbance flow will be tacitly identified with its leading-order component.

2.1. *Boundary integral formulation*

To compute the solution, we use the boundary integral formulation for Stokes flow. We begin by expressing the disturbance velocity at a point $\boldsymbol{x}_0$ that lies in the upper fluid labelled 1 in terms of integrals over the particle surface, P, and interface, I, as

$$\boldsymbol{u}^D(\boldsymbol{x}_0) = -\frac{1}{8\pi\mu_1}\mathscr{S}(\boldsymbol{x}_0, \boldsymbol{f}^D, P) - \frac{1}{8\pi\mu_1}\mathscr{S}\big(\boldsymbol{x}_0, \boldsymbol{f}_1^D, I\big) + \frac{1}{8\pi}\mathscr{D}(\boldsymbol{x}_0, \boldsymbol{u}^D, P) + \frac{1}{8\pi}\mathscr{D}(\boldsymbol{x}_0, \boldsymbol{u}^D, I). \quad (2.6)$$

We have introduced the single- and double-layer potentials of Stokes flow defined over a generic surface, D,

$$\left.\begin{aligned} \mathscr{S}_j(\boldsymbol{x}_0, \boldsymbol{f}, D) &\equiv \iint_D f_i(\boldsymbol{x})\, G_{ij}(\boldsymbol{x}, \boldsymbol{x}_0)\, \mathrm{d}S(\boldsymbol{x}), \\ \mathscr{D}_j(\boldsymbol{x}_0, \boldsymbol{u}, D) &\equiv \iint_D u_i(\boldsymbol{x})\, T_{ijk}(\boldsymbol{x}, \boldsymbol{x}_0)\, n_k(\boldsymbol{x})\, \mathrm{d}S(\boldsymbol{x}), \end{aligned}\right\} \quad (2.7)$$

where

$$G_{ij}(\boldsymbol{x}, \boldsymbol{x}_0) = \frac{\delta_{ij}}{r} + \frac{\hat{x}_i\hat{x}_j}{r^3}, \qquad T_{ijk}(\boldsymbol{x}, \boldsymbol{x}_0) = -6\frac{\hat{x}_i\hat{x}_j\hat{x}_k}{r^5}, \quad (2.8)$$

are the free-space Green's function and associated stress tensors, $\hat{\boldsymbol{x}} = \boldsymbol{x} - \boldsymbol{x}_0$, $r = |\hat{\boldsymbol{x}}|$, and δ_{ij} is Kronecker's delta (e.g. Pozrikidis 1992). Next, we apply the reciprocal identity for the simple shear flow in the upper fluid over the particle volume to obtain

$$\boldsymbol{0} = -\frac{1}{8\pi\mu_1}\mathscr{S}(\boldsymbol{x}_0, \boldsymbol{f}^\infty, P) + \frac{1}{8\pi}\mathscr{D}(\boldsymbol{x}_0, \boldsymbol{u}^\infty, P). \quad (2.9)$$

Adding (2.6) to (2.9), we find

$$\boldsymbol{u}^D(\boldsymbol{x}_0) = -\frac{1}{8\pi\mu_1}\mathscr{S}(\boldsymbol{x}_0, \boldsymbol{f}, P) - \frac{1}{8\pi\mu_1}\mathscr{S}\big(\boldsymbol{x}_0, \boldsymbol{f}_1^D, I\big) + \frac{1}{8\pi}\mathscr{D}(\boldsymbol{x}_0, \boldsymbol{u}, P) + \frac{1}{8\pi}\mathscr{D}(\boldsymbol{x}_0, \boldsymbol{u}^D, I). \quad (2.10)$$

Because the velocity over the particle surface expresses rigid-body motion, the penultimate integral on the right-hand side is zero, yielding the simplified representation

$$\boldsymbol{u}^D(\boldsymbol{x}_0) = -\frac{1}{8\pi\mu_1}\mathscr{S}(\boldsymbol{x}_0, \boldsymbol{f}, P) - \frac{1}{8\pi\mu_1}\mathscr{S}\big(\boldsymbol{x}_0, \boldsymbol{f}_1^D, I\big) + \frac{1}{8\pi}\mathscr{D}(\boldsymbol{x}_0, \boldsymbol{u}^D, I). \quad (2.11)$$

Now using the reciprocal theorem for the disturbance flow in the lower fluid, we find

$$\boldsymbol{0} = -\frac{1}{8\pi\mu_2}\mathscr{S}\big(\boldsymbol{x}_0, \boldsymbol{f}_2^D, I\big) + \frac{1}{8\pi}\mathscr{D}(\boldsymbol{x}_0, \boldsymbol{u}^D, I), \quad (2.12)$$

where $\boldsymbol{x}_0$ still lies in the upper fluid labelled 1. Combining (2.11) and (2.12) to form the jump in traction across the interface, $\Delta\boldsymbol{f}^D = \boldsymbol{f}_1^D - \boldsymbol{f}_2^D$, which is also equal to the jump in the physical traction, $\Delta\boldsymbol{f} = \boldsymbol{f}_1 - \boldsymbol{f}_2$, we find

$$\boldsymbol{u}^D(\boldsymbol{x}_0) = -\frac{1}{8\pi\mu_1}\mathscr{S}(\boldsymbol{x}_0, \boldsymbol{f}, P) - \frac{1}{8\pi\mu_1}\mathscr{S}(\boldsymbol{x}_0, \Delta\boldsymbol{f}, I) + \frac{1-\lambda}{8\pi}\mathscr{D}(\boldsymbol{x}_0, \boldsymbol{u}^D, I). \quad (2.13)$$

https://doi.org/10.1017/S0022112006004046 Published online by Cambridge University Press

For a point $\boldsymbol{x}_0$ located in the lower fluid we find an identical expression, except that the each term on the right-hand side is divided by the viscosity ratio, λ.

Applying (2.13) at the particle surface, enforcing the rigid-body-motion boundary condition and rearranging, we find

$$\mathscr{S}(\boldsymbol{x}_0, \boldsymbol{f}, P) + \mathscr{S}(\boldsymbol{x}_0, \Delta\boldsymbol{f}, I) - \mu_1(1-\lambda)\mathscr{D}(\boldsymbol{x}_0, \boldsymbol{u}^D, I) = -8\pi\mu_1 [\boldsymbol{V} + \boldsymbol{\Omega} \times (\boldsymbol{x}_0 - \boldsymbol{x}_c) - \boldsymbol{u}^\infty(\boldsymbol{x}_0)], \tag{2.14}$$

where the point $\boldsymbol{x}_0$ lies on P. Next, we take the limit of (2.13) as the evaluation point $\boldsymbol{x}_0$ approaches the interface, and use the identity

$$\lim_{\boldsymbol{x}_0 \to I} \mathscr{D}(\boldsymbol{x}_0, \boldsymbol{u}^D, I) = \mathscr{D}^{PV}(\boldsymbol{x}_0, \boldsymbol{u}^D, I) + 4\pi\boldsymbol{u}(\boldsymbol{x}_0), \tag{2.15}$$

where PV denotes the principal-value integral. The principal value of the double-layer potential is identically zero due to the vanishing of the kernel, T_{ijk}, yielding

$$\mathscr{S}(\boldsymbol{x}_0, \boldsymbol{f}, P) + \mathscr{S}(\boldsymbol{x}_0, \Delta\boldsymbol{f}, I) + 4\pi\mu_1(1+\lambda)\boldsymbol{u}^D(\boldsymbol{x}_0) = \boldsymbol{0}, \tag{2.16}$$

where the point $\boldsymbol{x}_0$ lies on I.

We have derived a system of six scalar equations for the three components of the traction over the particle surface, the normal component of the traction over the interface, and the two tangential components of the disturbance velocity over the interface. Solving these integral equations directly presents significant numerical challenges concerning the adequate discretization of the particle surface and interface and the accurate evaluation of the singular boundary integrals required in the boundary element method.

2.2. *Fourier expansion*

Because the interface is assumed to be virtually flat, the boundaries of the flow, but not the flow itself, are axially symmetric with respect to the x-axis. This geometrical property allows us to simplify the problem by expressing the cylindrical polar components of the left- and right-hand sides of (2.14) and (2.16) in Fourier series with respect to the meridional angle, φ, defined such that $y = \sigma\cos\varphi$ and $z = \sigma\sin\varphi$, as shown in figure 1(*a*), where σ is the distance from the x-axis. Since we are interested in a freely suspended particle, we set V_x, V_z, Ω_x, and Ω_y to zero and obtain

$$\boldsymbol{V} + \boldsymbol{\Omega} \times (\boldsymbol{x} - \boldsymbol{x}_c) - \boldsymbol{u}^\infty = -\Omega_z\sigma\cos\varphi\boldsymbol{e}_x + W(x)\cos\varphi\boldsymbol{e}_\sigma - W(x)\sin\varphi\boldsymbol{e}_\varphi, \tag{2.17}$$

where $\boldsymbol{e}_x$, $\boldsymbol{e}_\sigma$, $\boldsymbol{e}_\varphi$, are unit vectors, and

$$W(x) = V_y + \Omega_z(x - x_c) - u_y^\infty(x). \tag{2.18}$$

Motivated by this form, we express the velocity as

$$\boldsymbol{u} = \mathscr{V}_x\cos\varphi\boldsymbol{e}_x + \mathscr{V}_\sigma\cos\varphi\boldsymbol{e}_\sigma - \mathscr{V}_\varphi\sin\varphi\boldsymbol{e}_\varphi, \tag{2.19}$$

and the boundary traction as

$$\boldsymbol{f} = \mathscr{F}_x\cos\varphi\boldsymbol{e}_x + \mathscr{F}_\sigma\cos\varphi\boldsymbol{e}_\sigma - \mathscr{F}_\varphi\sin\varphi\boldsymbol{e}_\varphi, \tag{2.20}$$

where the coefficients $\mathscr{V}_\alpha$ and $\mathscr{F}_\alpha$ are functions of x and σ. The y component of the force and the z component of the torque exerted on the particle are given by

$$F_y = \pi\int_{C_P} (\mathscr{F}_\sigma + \mathscr{F}_\varphi)\sigma\,\mathrm{d}l, \qquad T_z = \pi\int_{C_P} ((x - x_c)(\mathscr{F}_\sigma + \mathscr{F}_\varphi) - \sigma\mathscr{F}_x)\sigma\,\mathrm{d}l, \tag{2.21}$$

https://doi.org/10.1017/S0022112006004046 Published online by Cambridge University Press

where C_P is the particle contour in the $\varphi = 0$ meridional plane consisting of half the xy plane, and l is the arclength along C_P. All other components of the force and torque are zero.

Substituting (2.20) in the cylindrical polar components of the single-layer potential and simplifying, we find

$$\begin{bmatrix} \mathscr{S}_x \\ \mathscr{S}_\sigma \\ \mathscr{S}_\varphi \end{bmatrix} (\boldsymbol{x}_0) = \int_{C_P} \begin{bmatrix} \cos\varphi_0(\Psi_{xx}\mathscr{F}_x + \Psi_{x\sigma}\mathscr{F}_\sigma + \Psi_{x\varphi}\mathscr{F}_\varphi) \\ \cos\varphi_0(\Psi_{\sigma x}\mathscr{F}_x + \Psi_{\sigma\sigma}\mathscr{F}_\sigma + \Psi_{\sigma\varphi}\mathscr{F}_\varphi) \\ -\sin\varphi_0(\Psi_{\varphi x}\mathscr{F}_x + \Psi_{\varphi\sigma}\mathscr{F}_\sigma + \Psi_{\varphi\varphi}\mathscr{F}_\varphi) \end{bmatrix} \mathrm{d}l. \tag{2.22}$$

Straightforward algebra yields the 3×3 kernel matrix

$$\Psi_{\alpha\gamma}(\boldsymbol{x}_0, \boldsymbol{x}) = \sigma \begin{bmatrix} \mathscr{I}_{11} + \hat{x}^2\mathscr{I}_{31} & \hat{x}(\sigma\mathscr{I}_{31} - \sigma_0\mathscr{I}_{32}) & \hat{x}\sigma_0(\mathscr{I}_{32} - \mathscr{I}_{30}) \\ \hat{x}(\sigma\mathscr{I}_{32} - \sigma_0\mathscr{I}_{31}) & \mathscr{I}_{12} + (\sigma^2 + \sigma_0^2)\mathscr{I}_{32} - \sigma\sigma_0(\mathscr{I}_{33} + \mathscr{I}_{31}) & \mathscr{I}_{10} - \mathscr{I}_{12} + \sigma^2(\mathscr{I}_{30} - \mathscr{I}_{32}) - \sigma\sigma_0(\mathscr{I}_{31} - \mathscr{I}_{33}) \\ \hat{x}\sigma(\mathscr{I}_{30} - \mathscr{I}_{32}) & \mathscr{I}_{10} - \mathscr{I}_{12} + \sigma_0^2(\mathscr{I}_{30} - \mathscr{I}_{32}) & \hat{x}\sigma(\mathscr{I}_{30} - \mathscr{I}_{32})\mathscr{I}_{12} + \sigma\sigma_0(\mathscr{I}_{31} - \mathscr{I}_{33}) \end{bmatrix}, \tag{2.23}$$

where

$$\mathscr{I}_{mn} = \int_0^{2\pi} \frac{\cos^n\omega\,\mathrm{d}\omega}{\left[\hat{x}^2 + \sigma^2 + \sigma_0^2 - 2\sigma\sigma_0\cos\omega\right]^{m/2}} = \frac{4w^m}{(4\sigma\sigma_0)^{m/2}} \int_0^{\pi/2} \frac{(2\cos^2\omega - 1)^n}{(1 - w^2\cos^2\omega)^{m/2}}\,\mathrm{d}\omega, \tag{2.24}$$

and $w^2 = 4\sigma\sigma_0/[\hat{x}^2 + (\sigma + \sigma_0)^2]$. These integrals can be expressed in terms of complete elliptic integrals of the first and second kind using standard mathematical tables. The elliptic integrals may then be evaluated with high accuracy using standard library functions or iterative methods.

Over the interface located at $x = 0$, the unit normal vector points along the x-axis and the double-layer potential takes the form

$$\begin{aligned} \mathscr{D}_j(\boldsymbol{x}_0, \boldsymbol{u}, I) &= -6\hat{x} \iint_I \frac{u_x\,\hat{x} + u_y\,\hat{y} + u_z\,\hat{z}}{\left[x_0^2 + \hat{y}^2 + \hat{z}^2\right]^{5/2}} (\boldsymbol{x} - \boldsymbol{x}_0)_j\,\mathrm{d}S(\boldsymbol{x}) \\ &= -6\hat{x} \iint_I \frac{u_x\,\hat{x} + u_\sigma\,(\sigma - \sigma_0\cos\hat{\varphi}) + u_\varphi\sigma_0\sin\hat{\varphi}}{\left(x_0^2 + \sigma^2 + \sigma_0^2 - 2\sigma\sigma_0\cos\hat{\varphi}\right)^{5/2}} (\boldsymbol{x} - \boldsymbol{x}_0)_j\,\mathrm{d}S(\boldsymbol{x}), \end{aligned} \tag{2.25}$$

where $\hat{\varphi} = \varphi - \varphi_0$. The associated cylindrical polar components are

$$\begin{bmatrix} \mathscr{D}_x \\ \mathscr{D}_\sigma \\ \mathscr{D}_\varphi \end{bmatrix} (\boldsymbol{x}_0, \boldsymbol{u}, I) = -6\hat{x} \iint_I \frac{u_x\,\hat{x} + u_\sigma\,(\sigma - \sigma_0\cos\hat{\varphi}) + u_\varphi\sigma_0\sin\hat{\varphi}}{\left(x_0^2 + \sigma^2 + \sigma_0^2 - 2\sigma\sigma_0\cos\hat{\varphi}\right)^{5/2}} \times \begin{bmatrix} \hat{x} \\ \sigma\cos\hat{\varphi} - \sigma_0 \\ \sigma\sin\hat{\varphi} \end{bmatrix} \mathrm{d}S(\boldsymbol{x}). \tag{2.26}$$

https://doi.org/10.1017/S0022112006004046 Published online by Cambridge University Press

Substituting (2.19) in (2.26) we obtain

$$\begin{bmatrix} \mathscr{D}_x \\ \mathscr{D}_\sigma \\ \mathscr{D}_\varphi \end{bmatrix}(\boldsymbol{x}_0) = \int_{C_I} \begin{bmatrix} \cos\varphi_0(K_{xx}\mathscr{V}_x + K_{x\sigma}\mathscr{V}_\sigma + K_{x\varphi}\mathscr{V}_\varphi) \\ \cos\varphi_0(K_{\sigma x}\mathscr{V}_x + K_{\sigma\sigma}\mathscr{V}_\sigma + K_{\sigma\varphi}\mathscr{V}_\varphi) \\ -\sin\varphi_0(K_{\varphi x}\mathscr{V}_x + K_{\varphi\sigma}\mathscr{V}_\sigma + K_{\varphi\varphi}\mathscr{V}_\varphi) \end{bmatrix} \mathrm{d}x, \tag{2.27}$$

where C_I is the trace of I in a meridional plane. Straightforward algebra yields the 3×3 kernel matrix

$$K_{\alpha\beta}(\boldsymbol{x}_0,\boldsymbol{x}) = -6\sigma\hat{x}\begin{bmatrix} \hat{x}^2\mathscr{I}_{51} & \hat{x}(\sigma\mathscr{I}_{51}-\sigma_0\mathscr{I}_{52}) & \hat{x}\sigma_0(\mathscr{I}_{52}-\mathscr{I}_{50}) \\ \hat{x}(\sigma\mathscr{I}_{52}-\sigma_0\mathscr{I}_{51}) & (\sigma^2+\sigma_0^2)\mathscr{I}_{52}-\sigma\sigma_0(\mathscr{I}_{51}+\mathscr{I}_{53}) & \sigma\sigma_0(\mathscr{I}_{53}-\mathscr{I}_{51})-\sigma_0^2(\mathscr{I}_{52}-\mathscr{I}_{50}) \\ \hat{x}\sigma(\mathscr{I}_{50}-\mathscr{I}_{52}) & \sigma^2(\mathscr{I}_{50}-\mathscr{I}_{52})+\sigma\sigma_0(\mathscr{I}_{53}-\mathscr{I}_{51}) & \sigma\sigma_0(\mathscr{I}_{51}-\mathscr{I}_{53}) \end{bmatrix}. \tag{2.28}$$

Substituting the expressions for the single- and double-layer potential in (2.13), we derive an integral representation for the Fourier coefficients,

$$\mathscr{V}_\alpha^D(\boldsymbol{x}_0) = -\frac{1}{8\pi\mu_1}\int_{C_P}\Psi_{\alpha\beta}(\boldsymbol{x}_0,\boldsymbol{x})\mathscr{F}_\beta(\boldsymbol{x})\,\mathrm{d}l(\boldsymbol{x}) - \frac{1}{8\pi\mu_1}\int_{C_I}\Psi_{\alpha\beta}(\boldsymbol{x}_0,\boldsymbol{x})\Delta\mathscr{F}_\beta(\boldsymbol{x})\,\mathrm{d}l(\boldsymbol{x}) + \frac{1-\lambda}{8\pi}\int_{C_I}K_{\alpha\delta}(\boldsymbol{x}_0,\boldsymbol{x})\mathscr{V}_\delta^D(\boldsymbol{x})\,\mathrm{d}l(\boldsymbol{x}), \tag{2.29}$$

where the point $\boldsymbol{x}_0$ lies in the upper fluid and δ runs over σ and φ. Substituting in (2.14), we obtain the integral equation

$$\int_{C_P}\Psi_{\alpha\beta}(\boldsymbol{x}_0,\boldsymbol{x})\mathscr{F}_\beta(\boldsymbol{x})\,\mathrm{d}l(\boldsymbol{x}) + \int_{C_I}\Psi_{\alpha\beta}(\boldsymbol{x}_0,\boldsymbol{x})\Delta\mathscr{F}_\beta(\boldsymbol{x})\,\mathrm{d}l(\boldsymbol{x}) - \mu_1(1-\lambda)\int_{C_I}K_{\alpha\delta}(\boldsymbol{x}_0,\boldsymbol{x})\mathscr{V}_\delta^D(\boldsymbol{x})\,\mathrm{d}l(\boldsymbol{x}) = -8\pi\mu_1(-\Omega_z\sigma_0\delta_{\alpha x} + W(\boldsymbol{x}_0)\delta_{\alpha\sigma} + W(\boldsymbol{x}_0)\delta_{\alpha\varphi}), \tag{2.30}$$

where the point $\boldsymbol{x}_0$ lies on C_P. Finally substituting in (2.15), we obtain the integral equation

$$\int_{C_P}\Psi_{\alpha\beta}(\boldsymbol{x}_0,\boldsymbol{x})\mathscr{F}_\beta(\boldsymbol{x})\,\mathrm{d}l(\boldsymbol{x}) + \int_{C_I}\Psi_{\alpha\beta}(\boldsymbol{x}_0,\boldsymbol{x})\Delta\mathscr{F}_\beta(\boldsymbol{x})\,\mathrm{d}l(\boldsymbol{x}) + 4\pi\mu_1(1+\lambda)\mathscr{V}_\alpha^D(\boldsymbol{x}_0) = 0,$$

where the point $\boldsymbol{x}_0$ lies on C_I. The boundary conditions require $\Delta\mathscr{F}_\sigma = 0$, $\Delta\mathscr{F}_\varphi = 0$ and $\mathscr{V}_x^D = 0$ over the interface.

The solution for the x component of the traction jump across the interface can be used to deduce the interfacial deformation to leading order with respect to the capillary number, Ca. Describing the interface as $x = a\,Ca\,\phi(y,z) = a\,Ca\cos\varphi\Phi(\sigma)$, and substituting in (2.5), we derive an inhomogeneous Bessel-like ordinary differential equation

$$\frac{1}{\sigma}\frac{\mathrm{d}}{\mathrm{d}\sigma}\left(\sigma\frac{\mathrm{d}\Phi}{\mathrm{d}\sigma}\right) - \frac{\Phi}{\sigma^2} = \frac{\mathrm{d}}{\mathrm{d}\sigma}\left(\frac{1}{\sigma}\frac{\mathrm{d}(\sigma\Phi)}{\mathrm{d}\sigma}\right) = -\frac{\Delta\mathscr{F}_x}{\mu_1 k_1 a^2}, \tag{2.31}$$

where Φ is a dimensionless function, and the right-hand side is known in numerical form. The boundary conditions specify the regularity and far-field conditions $\Phi(0) = 0$ and $\Phi(\infty) = 0$.

https://doi.org/10.1017/S0022112006004046 Published online by Cambridge University Press

2.3. *Numerical method*

To solve the integral equations, we divide the boundary contours in the $\varphi = 0$ meridional plane into straight elements over the interface and circular elements over the particle, and approximate the Fourier coefficients with constant functions over each element. For improved accuracy, the elements are concentrated near the axis of symmetry, with their length increasing geometrically with distance from the axis of symmetry, as depicted in figure 1(*b*). The interface is truncated at a radial distance equal to forty-eight times the particle separation from the interface, x_c. Next, we apply point collocation at the mid-point of each element and compile a system of linear equations for the unknown solution vector:

$$\left[(\mathscr{F}_x)_P(\Delta\mathscr{F}_x)_I\middle|(\mathscr{F}_\sigma)_P\left(\mathscr{V}_\sigma^D\right)_I\middle|(\mathscr{F}_\varphi)_P\left(\mathscr{V}_\varphi^D\right)_I\right], \tag{2.32}$$

where the vector block $(\mathscr{F}_x)_P$ contains the x component of the traction over the particle elements, and the rest of the blocks are defined in similar ways. The entries of the coefficient matrix are computed by the six-point Gauss–Legendre quadrature with special attention paid to the logarithmic singularity occurring at the diagonal components of the single-layer kernel, $\Psi_{\alpha\alpha}$. In the case of a freely suspended particle, the translational and angular velocities V_y and Ω_z are appended to the vector of unknowns, and two more equations are introduced expressing the vanishing of F_y and T_z. The solution of equation (2.31) is found by a standard finite volume method applied to the differential expression on the left-hand side.

The numerical method was validated by various tests and comparisons with the predictions of previous authors. In one case study, comparisons were made with the results of Lee & Leal (1980) who studied the translation and rotation of a spherical particle near the interface between two quiescent fluids by separation of variables in bipolar coordinates. Our computations for particle position $x_c/a = 1.1$ and viscosity ratio $\lambda = 10$ with 64 particle elements and 128 interfacial elements predict the reduced particle force and torque $F_y/(6\pi\mu_1 a V_y) = -1.820$ and $T_z/(8\pi\mu_1 a^2 V_y) = 0.0192$. These values compare favourably with those given in table 2 and 3 of the previous authors, respectively, -1.82067 and 0.0192084. For $x_c/a = 1.2$ and $\lambda = 0.1$ and same number of boundary elements, we find the reduced force and torque -0.796 and -0.0896, which agree well with the values -0.795140 and -0.0892500 reported by the previous authors. The numerical results discussed in the remainder of this section are estimated to carry an error on the order of ± 0.001.

2.4. *Results and discussion*

As a preliminary, we consider flow past a spherical particle that is held stationary in simple shear flow above the interface. Figure 2(*a*, *b*) shows the distribution of the traction coefficients along the particle contour and the distribution of the disturbance traction and velocity coefficients along the interface for $x_c/a = 1.1276$ and viscosity ratio $\lambda = 5$. The traction coefficients have been reduced by $\mu_1 k_1$, and the velocity coefficients have been reduced by $k_1 a$. The solid lines representing the x Fourier coefficient tend to zero at the axis of symmetry in both graphs, while the corresponding σ and φ coefficients tend to common limits, as required for a single-valued solution. Figure 2(*c*) illustrates the velocity vector field over the interface, showing the occurrence of backflow, and figure 2(*d*) illustrates the deformation of the interface computed by solving the Bessel-like equation derived in the previous section. We observe the formation of a localized peak and a localized depression, respectively, upstream and downstream of the particle centre. Figure 3 shows corresponding results for a fluid pair with low viscosity ratio, $\lambda = 0.1$. Although the general features of the

https://doi.org/10.1017/S0022112006004046 Published online by Cambridge University Press

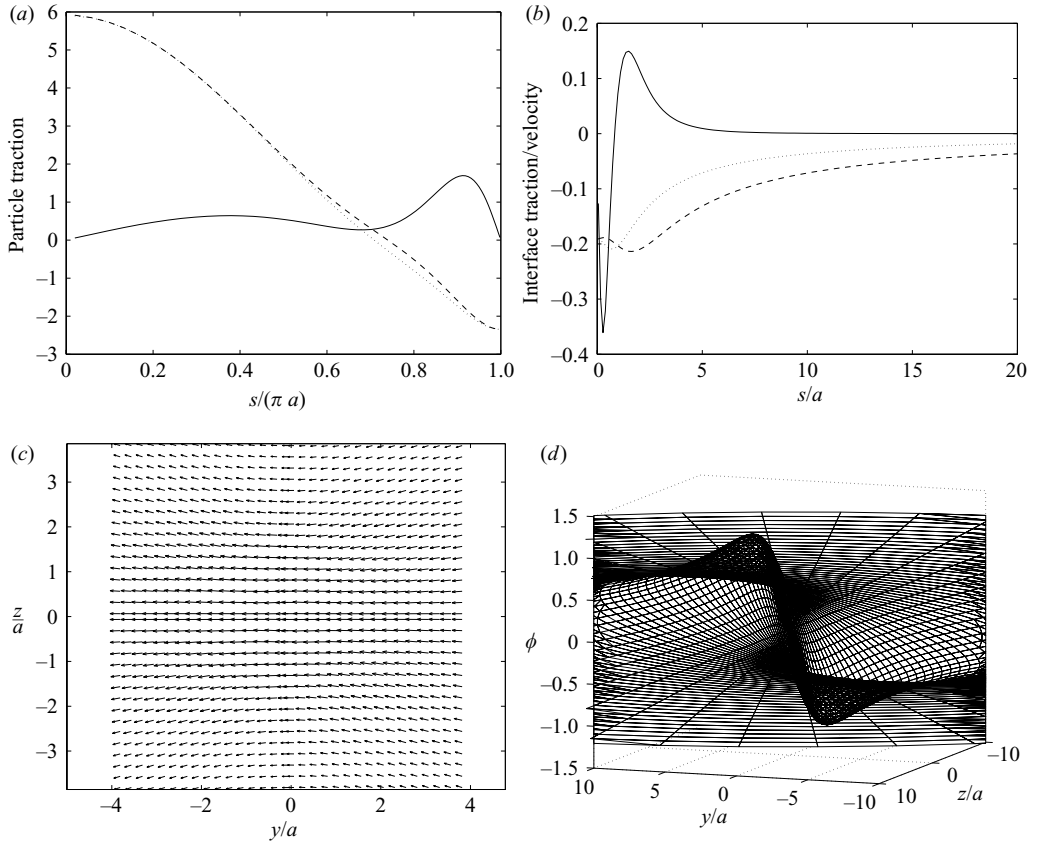


FIGURE 2. Shear flow past a spherical particle held stationary at a distance $x_c/a = 1.1276$ above the interface, for viscosity ratio $\lambda = 5$. (*a*) Distribution of the particle traction coefficients $\mathscr{F}_x$ (solid line), $\mathscr{F}_\sigma$ (dashed line), $\mathscr{F}_\varphi$ (dotted line), with respect to arclength measured from the axis of symmetry farthest from the wall. (*b*) Distribution of the interface traction coefficient $(1/5)\Delta\mathscr{F}_x^D$ (solid line), and velocity coefficients $\mathscr{V}_\sigma^D$ (dashed line), $\mathscr{V}_\varphi^D$ (dotted line), with respect to arclength measured from the axis of symmetry. (*c*) Disturbance velocity vector field over the interface, and (*d*) deformed shape of the interface.

flow are similar to those presented in figure 2 for the high viscosity ratio, close inspection reveals that the disturbance flow spreads over a greater distance owing to the increased mobility of the lower fluid.

The dimensionless force exerted on the particle is defined as $\hat{F}_y \equiv F_y/(6\pi\mu_1 k_1 x_c a)$, and the dimensionless torque is defined as $\hat{T}_z \equiv T_z/(4\pi\mu_1 k_1 a^3)$. Numerical results for $x_c/a = 1.1276$ are shown in table 1 for a range of viscosity ratios. As $\lambda \to \infty$, the two sequences converge to limits identified by Goldman, Cox & Brenner (1967) for a sphere held stationary in shear flow above a plane wall. The symbols in figure 4(*a*) trace the graph of the computed force and torque, both reduced by the limiting values for $\lambda = \infty$, plotted against the parameter $(1-\lambda)/(1+\lambda)$, which varies in the finite range $[-1, 1]$. We observe that the force exhibits a mild dependence, whereas the torque exhibits a much stronger dependence on the viscosity ratio. As λ tends to zero, the force and torque tend to well-defined limits corresponding to motion near a free surface.

https://doi.org/10.1017/S0022112006004046 Published online by Cambridge University Press

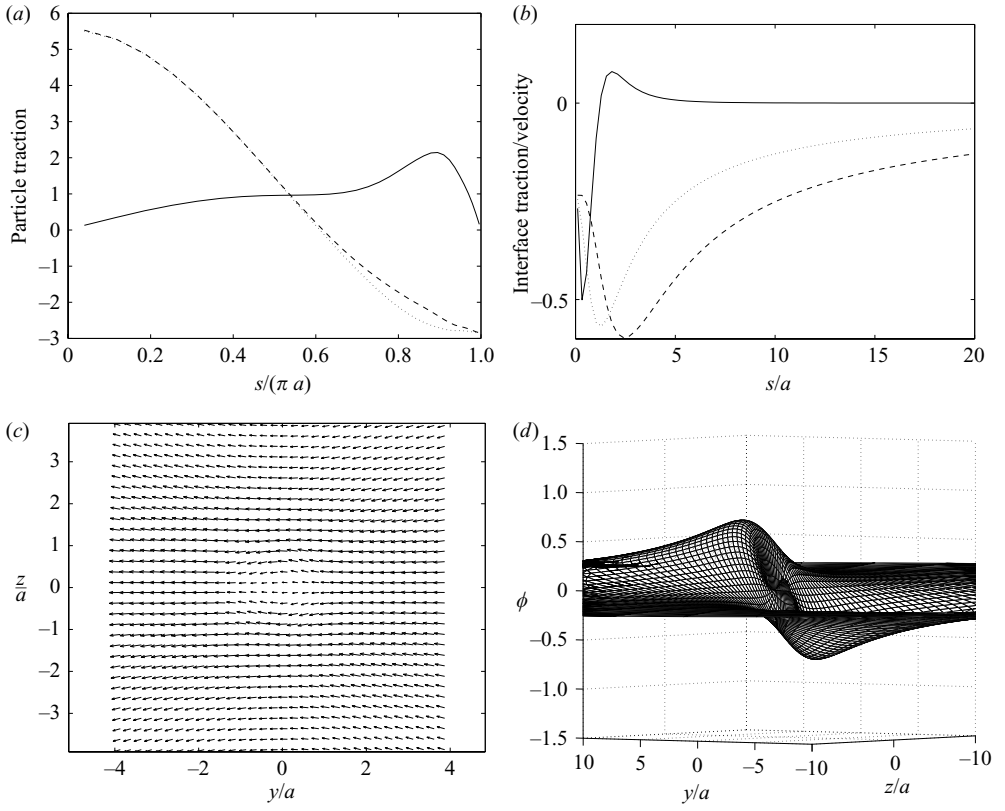


FIGURE 3. As figure 2 but for $\lambda = 0.1$.

λ	0.1	0.5	1	2.3	5	10	50	100	500	1000	∞
$\hat{F}_y$	0.850	0.939	1.021	1.159	1.305	1.419	1.565	1.589	1.610	1.612	1.6160
$\hat{T}_z$	0.999	1.019	1.028	1.030	1.017	0.998	0.967	0.961	0.956	0.956	0.95374

TABLE 1. Dimensionless force, $\hat{F}_y \equiv F_y/(6\pi\mu_1 k_1 x_c a)$, and dimensionless torque, $\hat{T}_z \equiv T_z/(4\pi\mu_1 k_1 a^3)$, exerted on a spherical particle that is held stationary at a distance $x_c/a = 1.1276$ above the interface in simple shear flow, listed as a function of the viscosity ratio. When the viscosity ratio is infinite, the particle is suspended in simple shear flow above a plane wall.

Yang & Leal (1984) determined that the force and torque exerted on a small sphere far from the interface are given by the asymptotic expansions

$$\left.\begin{aligned} \hat{F}_y &= 1 - \Delta + \Delta^2 - \Delta^3 - \frac{1+2\lambda}{16(1+\lambda)}\delta^3 + \delta^2\frac{2-5\lambda}{16(1+\lambda)}(1-\Delta) + O(\delta^4), \\ \hat{T}_z &= 1 + \frac{3}{8}\frac{\delta}{1+\lambda}(1-\Delta-\delta^2) + O(\delta^4), \end{aligned}\right\} \tag{2.33}$$

where $\delta = a/x_c$, $\Delta = \alpha\delta$, and $\alpha = 3(2-3\lambda)/[16(1+\lambda)]$. Note that, as $\lambda \to \infty$, the correction to the torque becomes at least quartic with respect to δ, and is therefore inadequately described by the third-order perturbation expansion. The dashed and

https://doi.org/10.1017/S0022112006004046 Published online by Cambridge University Press

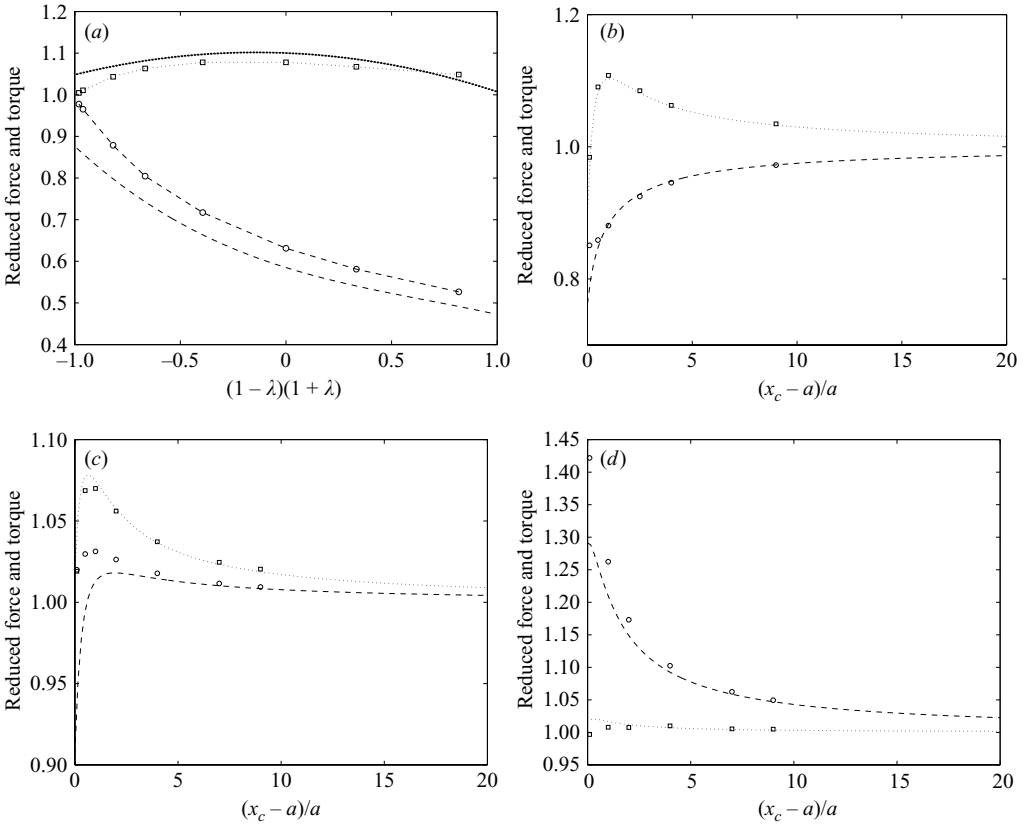


FIGURE 4. (*a*) Force, F_y, (circles and dashed lines), and torque, T_z, (squares and dotted lines), exerted on a sphere held stationary above an interface at a distance $x_c/a = 1.1276$ in simple shear flow, reduced by the corresponding values for an immobilized lower fluid, $\lambda = \infty$. (*b–d*) Reduced force $\hat{F}_y$ (circles) and torque $\hat{T}_z$ (squares) plotted against the particle distance from the interface for (*b*) $\lambda = 0.1$, (*c*) 1, and (*d*) 10. In all graphs, the dotted and dashed lines without symbols represent the asymptotic predictions for distant particles.

dotted lines without symbols in figure 4(*a*) represent these asymptotic predictions. The deviation of the asymptotic from the numerical results is surprisingly small considering that the particle is so close to the interface. Figures 4(*b*), 4(*c*) and 4(*d*) display our numerical results for the force and torque plotted against the particle centre position for viscosity ratios $\lambda = 0.1$, 1, and 10. The agreement between these results and the asymptotic predictions represented by the dashed and dotted lines is good even for small particle-to-interface separations.

Next, we consider the velocity of translation and angular velocity of rotation of a freely suspended particle. Figures 5 and 6 illustrate the distribution of the traction along the particle contour, the distribution of the disturbance traction and velocity along the interface, the velocity vector field over the interface, and the deformation of the interface, for $x_c/a = 2$ and $\lambda = 5$ and 0.1. The traction coefficients have been reduced by $\mu_1 k_1$, and the velocity coefficients have been reduced by $k_1 a$. The viscosity ratio has an important effect on the distribution of traction and velocity over the interface, and the structure of the flow differs substantially from that described previously for a stationary particle. However, as in the case of the stationary particle,

https://doi.org/10.1017/S0022112006004046 Published online by Cambridge University Press

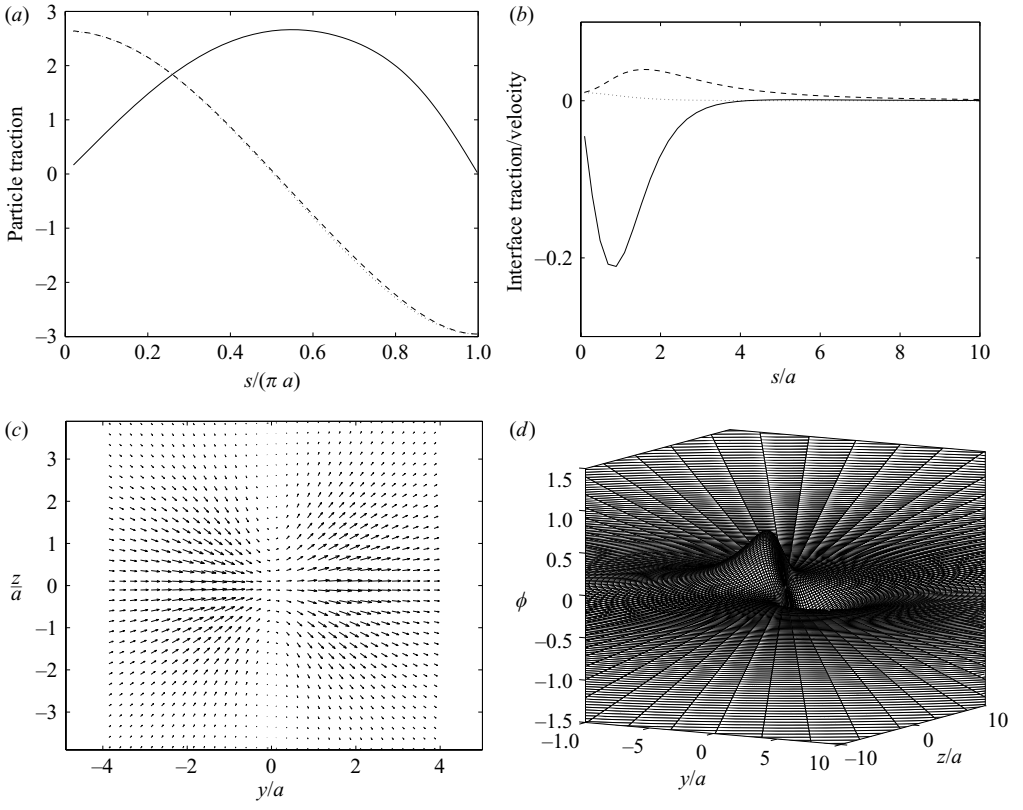


FIGURE 5. Flow past a freely suspended particle located at a distance $x_c/a = 2$ above the interface, for viscosity ratio $\lambda = 5$. (*a*) Distribution of the particle traction coefficients $\mathscr{F}_x$ (solid line), $\mathscr{F}_\sigma$ (dashed line), $\mathscr{F}_\varphi$ (dotted line), plotted with respect to arclength measured from the axis of symmetry farthest from the wall. (*b*) Distribution of the interface traction coefficient $(1/5)\Delta\mathscr{F}_x^D$ (solid line), and velocity coefficients $\mathscr{V}_\sigma^D$ (dashed line), $\mathscr{V}_\varphi^D$ (dotted line), plotted with respect to arclength measured from the axis of symmetry. (*c*) Disturbance velocity vector field over the interface, and (*d*) deformed shape of the interface.

an interfacial peak and a depression develop, respectively, upstream and downstream of the particle centre.

Computations for $x_c/a = 1.1276$ and a sequence of viscosity ratios yielded the values for the translational and angular velocities given in table 2. As $\lambda \to \infty$, the two sequences converge to limits identified by Goldman *et al.* (1967) for a spherical particle above a solid wall. The circles and squares in figure 7(*a*) trace the graphs of the computed linear and angular velocities reduced by the respective values for a solid wall, plotted against the parameter $(\lambda - 1)/(\lambda + 1)$. The translational velocity exhibits a strong dependence, whereas the angular velocity exhibits a mild dependence on the viscosity ratio. As $\lambda \to 0$, the velocities tend to well-defined limits corresponding to motion near a free surface.

The circles and squares in figures 7(*b*), 7(*c*) and 7(*d*) represent our numerical results for viscosity ratios $\lambda = 0.1$, 1, and 10. For small distances from the interface, the reduced rate of rotation for $\lambda = 0.1$ shown in panel (*b*) rises to become higher than that in an infinite fluid, $2\Omega_z/k > 1$. The numerical results for $\lambda = 10$ shown in panel (*d*) are in excellent agreement with the analytical predictions of Goldman

https://doi.org/10.1017/S0022112006004046 Published online by Cambridge University Press

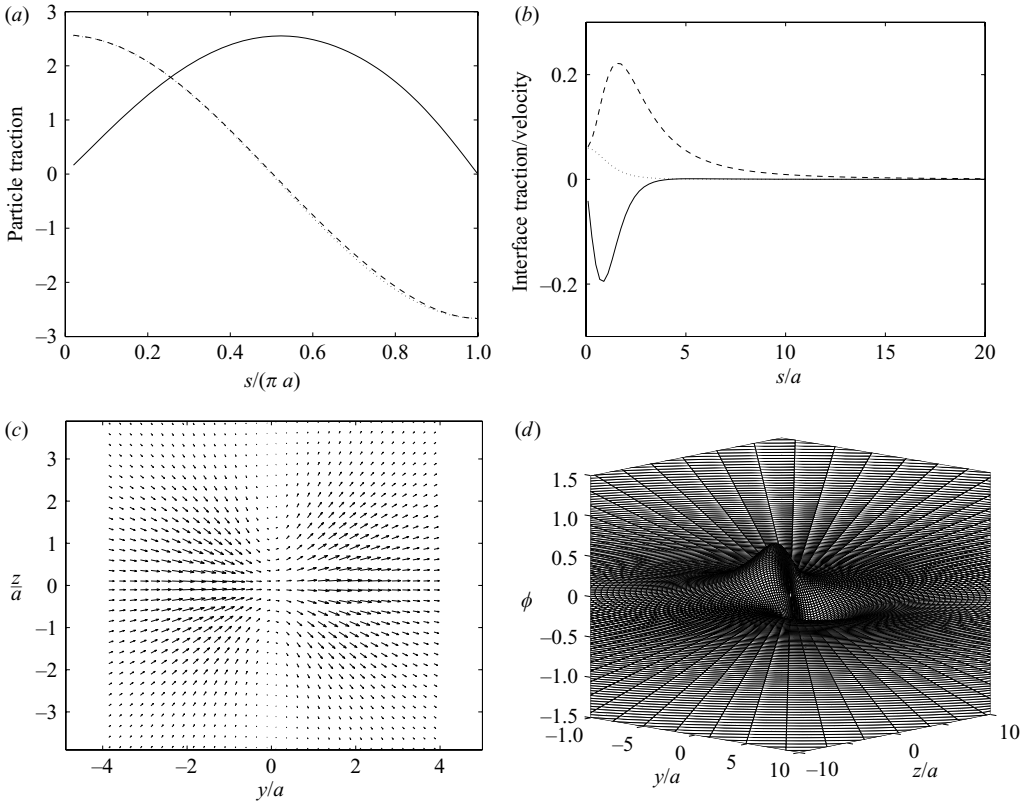


FIGURE 6. Same as figure 5 but for $\lambda = 0.01$.

λ	0.1	0.5	1	2.3	5	10	50	100	500	1000	∞
V_y/U_c	1.029	0.979	0.939	0.882	0.836	0.807	0.776	0.772	0.768	0.767	0.76692
$2\,\Omega_z/k$	0.722	0.731	0.740	0.752	0.763	0.770	0.778	0.779	0.780	0.780	0.77916

TABLE 2. Translational and rotational velocities of a freely suspended particle placed at a distance $x_c/a = 1.1276$ above the interface, listed as a function of the viscosity ratio; U_c is the velocity of the unperturbed simple shear flow evaluated at the particle centre.

et al. (1967) represented by the asterisks and crosses, respectively, for the force and torque, applicable in the limit $\lambda \to \infty$. These authors found that the ratios V_y/U_c and $2\Omega_z/k$ both drop to zero when the particle is tangential to a wall, exhibiting a sharp decline from the approximate values of 0.45 and 0.48 at $y_c/a = 1.003$. Thus, a spherical particle resting on the wall is immobilized by strong lubrication forces. The present results demonstrate non-zero limits for finite viscosity ratios. To assess whether a particle rolls over the interface without slipping, we examine whether the limit of the ratio $a\Omega_z/V_y$ represented by the diamonds in figure 7 tends to unity as $y_c \to a$. Goldman *et al.* (1967) found that this ratio tends to 0.5676 for flow over a solid wall. Our results demonstrate lower values for finite viscosity ratios, revealing a substantial slip velocity.

https://doi.org/10.1017/S0022112006004046 Published online by Cambridge University Press

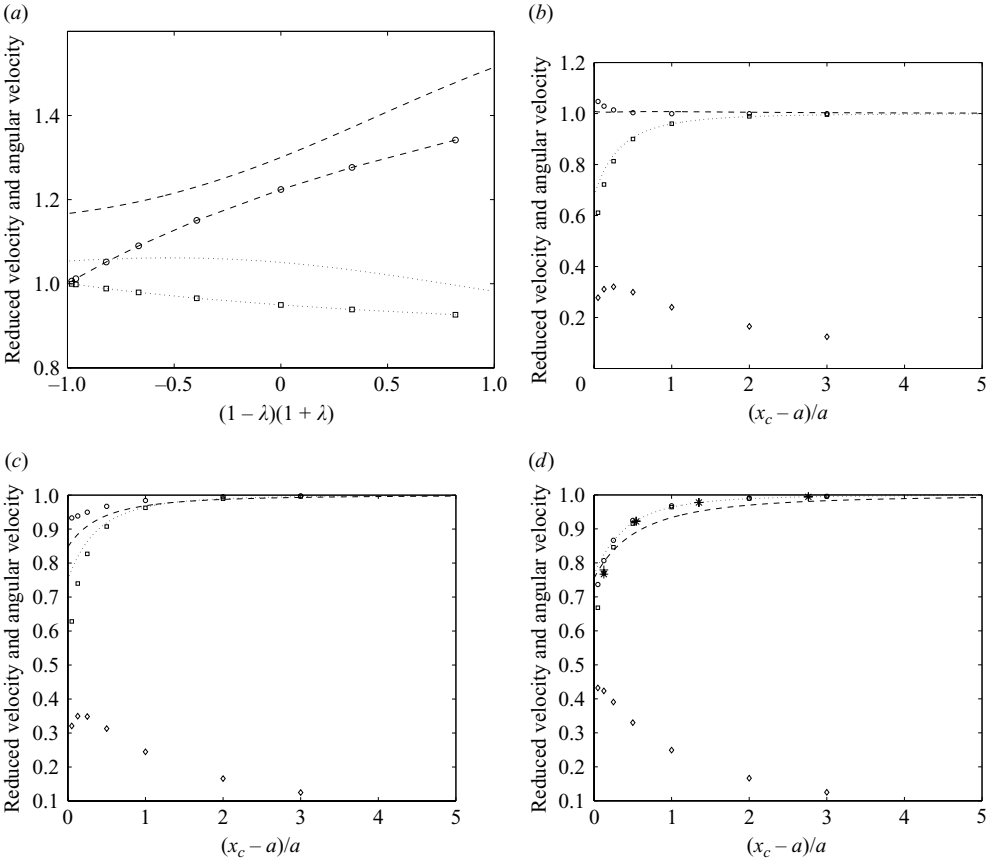


FIGURE 7. (*a*) Velocity of translation (circles and dashed lines) and angular velocity of rotation (squares and dotted lines) of a freely suspended particle located at the distance $x_c/a = 1.1276$ above the interface. The symbols connected by lines show the present numerical results, and the lines without symbols represent the asymptotic predictions of Yang & Leal (1984). The velocities are scaled by the corresponding values for motion above a plane wall, $\lambda = \infty$. (*b–d*) Reduced velocity of translation V_y/U_c (circles) and angular velocity of rotation $2\Omega_z/k$ (squares) for (*b*) $\lambda = 0.1$, (*c*) 1, and (*d*) 10. In all graphs, the dotted and dashed lines without symbols represent the asymptotic predictions for distant particles. The diamonds represent the ratio $a\Omega_z/V_y$, considered to assess whether a particle rolls or slips over the interface. In (*d*), the asterisks and nearly coincident crosses represent the predictions of Goldman *et al.* (1967) for V_y and Ω_z, prevailing in the limit $\lambda \to \infty$.

Lee, Chadwick & Leal (1979) and Yang & Leal (1984) determined the force and torque exerted on a sphere executing rigid-body motion far from the interface in a quiescent environment. Their predictions for a sphere translating along the y axis with velocity V_y while rotating about the z axis with angular velocity Ω_z are

$$\left.\begin{aligned} F_y &= -6\pi\mu a V_y\left(1-\Delta+\Delta^2-\Delta^3-\frac{1+2\lambda}{16(1+\lambda)}\delta^3\right)-\delta^2\frac{3\pi\mu a^2}{2(1+\lambda)}\Omega_z(1-\Delta)+O(\delta^4),\\ T_z &= -\delta^2\frac{3\pi\mu a^2}{2(1+\lambda)}V_y(1-\Delta)-8\pi\mu a^3\Omega_z\left(1+\frac{\delta^3}{16}\frac{5\lambda-1}{\lambda+1}\right)+O(\delta^4). \end{aligned}\right\} \tag{2.34}$$

https://doi.org/10.1017/S0022112006004046 Published online by Cambridge University Press

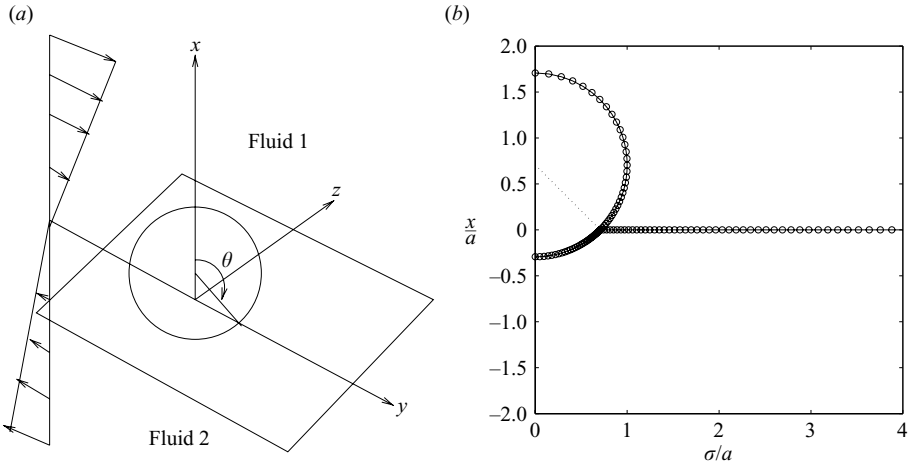


FIGURE 8. (*a*) A spherical particle straddling the interface between two immiscible viscous fluids. (*b*) Typical discretization of the particle and interface contour in an azimuthal plane for $\theta = 0.65\pi$.

These asymptotic results complement the numerical results of Lee & Leal (1980) for arbitrary particle positions. Combining (2.34) with (2.33) and imposing the condition of zero force and torque, we may deduce the velocity of translation and angular velocity of rotation of a freely-suspended particle by solving a system of two linear equations. The asymptotic predictions represented by the dashed and dotted lines without symbols in figure 7(*a*) provide only fair estimates due to the small separation of the particle from the interface. The graphs in figure 7(*b*, *c*) for $\lambda = 0.1$ and 1.0 show that the asymptotic predictions are in good agreement with the numerical results for large and moderate particle positions, whereas the graphs in figure 7(*d*) for $\lambda = 10$ show that the differences are significant even at large particle separations. The reason is that, in the limit $\lambda \to \infty$, the asymptotic analysis does not capture the leading-order correction to the force due to rotation or torque due to translation.

3. Particle embedded in an interface

In the second part of this paper, we consider the motion of a spherical particle straddling the interface between two immiscible fluids in the presence of a simple shear flow, as illustrated in figure 8. The level of particle penetration is determined by the azimuthal angle θ measured around the particle centre in a meridional plane up to the three-phase contact line, varying in the range $[0, \pi]$, as shown in figure 8(*a*); $\theta = \pi$ and 0 correspond, respectively, to a particle positioned in the upper or lower fluid tangentially to the interface. If the fluids have equal densities and the particle is neutrally buoyant, θ is determined by the contact angle at the three-phase contact line. Under more general conditions, a curved meniscus develops around the contact angle, and the angle θ is determined by the densities of the fluid and particle materials. In our analysis, we will assume that all densities are equal and surface tension is sufficiently strong to prevent significant interfacial deformation after the motion has been established.

https://doi.org/10.1017/S0022112006004046 Published online by Cambridge University Press

3.1. *Boundary integral formulation*

We begin by developing the boundary integral representation for a translating, rotating, and freely convected particle. The integral representation of the disturbance velocity at a point $\boldsymbol{x}_0$ that lies in the upper fluid is

$$\begin{aligned}\boldsymbol{u}^D(\boldsymbol{x}_0) = &-\frac{1}{8\pi\mu_1}\mathscr{S}(\boldsymbol{x}_0, \boldsymbol{f}^D, P_1) + \frac{1}{8\pi}\mathscr{D}(\boldsymbol{x}_0, \boldsymbol{u}^D, P_1)\\ &-\frac{1}{8\pi\mu_1}\mathscr{S}\big(\boldsymbol{x}_0, \boldsymbol{f}_1^D, I\big) + \frac{1}{8\pi}\mathscr{D}(\boldsymbol{x}_0, \boldsymbol{u}^D, I),\end{aligned} \tag{3.1}$$

where P_1 is the particle surface exposed to fluid 1. The reciprocal identity for the flow in the lower fluid requires

$$\begin{aligned}\boldsymbol{0} = &-\frac{1}{8\pi\mu_2}\mathscr{S}(\boldsymbol{x}_0, \boldsymbol{f}^D, P_2) + \frac{1}{8\pi}\mathscr{D}(\boldsymbol{x}_0, \boldsymbol{u}^D, P_2)\\ &+\frac{1}{8\pi\mu_2}\mathscr{S}\big(\boldsymbol{x}_0, \boldsymbol{f}_2^D, I\big) - \frac{1}{8\pi}\mathscr{D}(\boldsymbol{x}_0, \boldsymbol{u}^D, I),\end{aligned} \tag{3.2}$$

where P_2 is the particle surface exposed to fluid 2. Combining (3.1) and (3.2) to formulate the jump in the traction across the interface, we find

$$\begin{aligned}\boldsymbol{u}^D(\boldsymbol{x}_0) = &-\frac{1}{8\pi\mu_1}\mathscr{S}(\boldsymbol{x}_0, \boldsymbol{f}^D, P) + \frac{1}{8\pi}\mathscr{D}(\boldsymbol{x}_0, \boldsymbol{u}^D, P_1) + \frac{\lambda}{8\pi}\mathscr{D}(\boldsymbol{x}_0, \boldsymbol{u}^D, P_2)\\ &-\frac{1}{8\pi\mu_1}\mathscr{S}(\boldsymbol{x}_0, \Delta\boldsymbol{f}, I) + \frac{1-\lambda}{8\pi}\mathscr{D}(\boldsymbol{x}_0, \boldsymbol{u}^D, I).\end{aligned} \tag{3.3}$$

Since the stress field of the incident simple shear flow is common in both fluids, and since the velocity satisfies $\lambda\boldsymbol{u}^{\infty,2} = \boldsymbol{u}^{\infty,1}$, we may write the reciprocal identity

$$\boldsymbol{0} = -\frac{1}{8\pi\mu_1}\mathscr{S}(\boldsymbol{x}_0, \boldsymbol{f}^\infty, P) + \frac{1}{8\pi}\mathscr{D}(\boldsymbol{x}_0, \boldsymbol{u}^{\infty,1}, P_1) + \frac{\lambda}{8\pi}\mathscr{D}(\boldsymbol{x}_0, \boldsymbol{u}^{\infty,2}, P_2). \tag{3.4}$$

Combining the last two equations, we find

$$\begin{aligned}\boldsymbol{u}(\boldsymbol{x}_0) = \boldsymbol{u}^{\infty,1}(\boldsymbol{x}_0) &-\frac{1}{8\pi\mu_1}\mathscr{S}(\boldsymbol{x}_0, \boldsymbol{f}, P) + \frac{1}{8\pi}\mathscr{D}(\boldsymbol{x}_0, \boldsymbol{u}, P_1) + \frac{\lambda}{8\pi}\mathscr{D}(\boldsymbol{x}_0, \boldsymbol{u}, P_2)\\ &-\frac{1}{8\pi\mu_1}\mathscr{S}(\boldsymbol{x}_0, \Delta\boldsymbol{f}, I) + \frac{1-\lambda}{8\pi}\mathscr{D}(\boldsymbol{x}_0, \boldsymbol{u}^D, I),\end{aligned} \tag{3.5}$$

where the point $\boldsymbol{x}_0$ lies in the upper fluid. Working in a similar fashion for a point $\boldsymbol{x}_0$ that lies in the lower fluid we find an identical expression, except that the left-hand side is multiplied by the viscosity ratio, λ.

To derive integral equations, we take the limit of (3.5) as the point $\boldsymbol{x}_0$ approaches the upper particle surface, P_1, and enforce the slip boundary condition to find

$$\begin{aligned}&\mathscr{S}(\boldsymbol{x}_0, \boldsymbol{f}, P) - \mu_1\mathscr{D}^{PV}(\boldsymbol{x}_0, \boldsymbol{u}, P_1) - \lambda\mu_1\mathscr{D}(\boldsymbol{x}_0, \boldsymbol{u}, P_2) + \mathscr{S}(\boldsymbol{x}_0, \Delta\boldsymbol{f}, I)\\ &\quad-\mu_1(1-\lambda)\mathscr{D}(\boldsymbol{x}_0, \boldsymbol{u}^D, I) = -4\pi\mu_1[\boldsymbol{u}(\boldsymbol{x}_0) - 2\,\boldsymbol{u}^{\infty,1}(\boldsymbol{x}_0)],\end{aligned} \tag{3.6}$$

where PV denotes the principal value of the double-layer integral. For a point $\boldsymbol{x}_0$ located at the lower part, P_2, we find

$$\begin{aligned}&\mathscr{S}(\boldsymbol{x}_0, \boldsymbol{f}, P) - \mu_1\mathscr{D}(\boldsymbol{x}_0, \boldsymbol{u}, P_1) - \lambda\mu_1\mathscr{D}^{PV}(\boldsymbol{x}_0, \boldsymbol{u}, P_2) + \mathscr{S}(\boldsymbol{x}_0, \Delta\boldsymbol{f}, I)\\ &\quad-\mu_1(1-\lambda)\mathscr{D}(\boldsymbol{x}_0, \boldsymbol{u}^D, I) = -4\pi\lambda\,\mu_1[\boldsymbol{u}(\boldsymbol{x}_0) - 2\,\boldsymbol{u}^{\infty,2}(\boldsymbol{x}_0)].\end{aligned} \tag{3.7}$$

https://doi.org/10.1017/S0022112006004046 Published online by Cambridge University Press

Finally, for a point $\boldsymbol{x}_0$ located at the interface, we find

$$\mathscr{S}(\boldsymbol{x}_0, \boldsymbol{f}, P) - \mu_1 \mathscr{D}(\boldsymbol{x}_0, \boldsymbol{u}, P_1) - \lambda\mu_1 \mathscr{D}(\boldsymbol{x}_0, \boldsymbol{u}, P_2) + \mathscr{S}(\boldsymbol{x}_0, \Delta\boldsymbol{f}, I) + 4\pi\mu_1(1+\lambda)\boldsymbol{u}^D(\boldsymbol{x}_0) = \boldsymbol{0}. \tag{3.8}$$

If the boundary conditions on the particle specify rigid-body motion (RBM), we may use an integral identity to write

$$\left.\begin{aligned} \mathscr{D}^{PV}(\boldsymbol{x}_0, \boldsymbol{u}^{RBM}, P_1) &= -4\pi\boldsymbol{u}^{RBM}(\boldsymbol{x}_0) + \mathscr{D}(\boldsymbol{x}_0, \boldsymbol{u}^{RBM}, B), \\ \mathscr{D}(\boldsymbol{x}_0, \boldsymbol{u}^{RBM}, P_2) &= -\mathscr{D}(\boldsymbol{x}_0, \boldsymbol{u}^{RBM}, B), \end{aligned}\right\} \tag{3.9}$$

when $\boldsymbol{x}_0$ lies on P_1,

$$\left.\begin{aligned} \mathscr{D}^{PV}(\boldsymbol{x}_0, \boldsymbol{u}^{RBM}, P_2) &= -4\pi\boldsymbol{u}^{RBM}(\boldsymbol{x}_0) - \mathscr{D}(\boldsymbol{x}_0, \boldsymbol{u}^{RBM}, B), \\ \mathscr{D}(\boldsymbol{x}_0, \boldsymbol{u}^{RBM}, P_1) &= \mathscr{D}(\boldsymbol{x}_0, \boldsymbol{u}^{RBM}, B), \end{aligned}\right\} \tag{3.10}$$

when $\boldsymbol{x}_0$ lies on P_2, and

$$\left.\begin{aligned} \mathscr{D}(\boldsymbol{x}_0, \boldsymbol{u}^{RBM}, P_1) &= \mathscr{D}(\boldsymbol{x}_0, \boldsymbol{u}^{RBM}, B) = 0, \\ \mathscr{D}(\boldsymbol{x}_0, \boldsymbol{u}^{RBM}, P_2) &= -\mathscr{D}(\boldsymbol{x}_0, \boldsymbol{u}^{RBM}, B) = 0, \end{aligned}\right\} \tag{3.11}$$

when $\boldsymbol{x}_0$ lies on I, where B is the discoidal surface enclosed by the circular contact line, and the normal vector $\boldsymbol{n}$ over B points into the upper fluid. Substituting in (3.6), (3.7), and (3.8) to eliminate the integrals over the particles in favour of integrals over the discoidal surface, we obtain

$$\mathscr{S}(\boldsymbol{x}_0, \boldsymbol{f}, P) + \mathscr{S}(\boldsymbol{x}_0, \Delta\boldsymbol{f}, I) - \mu_1(1-\lambda)\mathscr{D}(\boldsymbol{x}_0, \boldsymbol{u}^D, I) = \mu_1(1-\lambda)\mathscr{D}(\boldsymbol{x}_0, \boldsymbol{u}^{RBM}, B) - 8\pi\mu_1[\boldsymbol{u}^{RBM}(\boldsymbol{x}_0) - \boldsymbol{u}^{\infty,1}(\boldsymbol{x}_0)], \tag{3.12}$$

when $\boldsymbol{x}_0$ lies on P_1,

$$\mathscr{S}(\boldsymbol{x}_0, \boldsymbol{f}, P) + \mathscr{S}(\boldsymbol{x}_0, \Delta\boldsymbol{f}, I) - \mu_1(1-\lambda)\mathscr{D}(\boldsymbol{x}_0, \boldsymbol{u}^D, I) = \mu_1(1-\lambda)\mathscr{D}(\boldsymbol{x}_0, \boldsymbol{u}^{RBM}, B) - 8\pi\lambda\mu_1[\boldsymbol{u}^{RBM}(\boldsymbol{x}_0) - \boldsymbol{u}^{\infty,2}(\boldsymbol{x}_0)], \tag{3.13}$$

when $\boldsymbol{x}_0$ lies on P_2, and

$$\mathscr{S}(\boldsymbol{x}_0, \boldsymbol{f}, P) + \mathscr{S}(\boldsymbol{x}_0, \Delta\boldsymbol{f}, I) + 4\pi\mu_1(1+\lambda)\boldsymbol{u}^D(\boldsymbol{x}_0) = \boldsymbol{0}, \tag{3.14}$$

when $\boldsymbol{x}_0$ lies on I. We have derived a system of integral equations for the traction over the particle surface, the x-component of the traction over the interface, and the tangential components of the disturbance velocity over the interface.

Now implementing the Fourier expansions as discussed in § 2, we obtain the one-dimensional equations

$$\int_{C_P} \Psi_{\alpha\beta}(\boldsymbol{x}_0, \boldsymbol{x})\mathscr{F}_\beta(\boldsymbol{x})\,\mathrm{d}l(\boldsymbol{x}) + \int_{C_I} \Psi_{\alpha\beta}(\boldsymbol{x}_0, \boldsymbol{x})\Delta\mathscr{F}_\beta(\boldsymbol{x})\,\mathrm{d}l(\boldsymbol{x}) - \mu_1(1-\lambda)\int_{C_I} K_{\alpha\delta}(\boldsymbol{x}_0, \boldsymbol{x})\mathscr{V}_\delta^D(\boldsymbol{x})\,\mathrm{d}l(\boldsymbol{x}) = \mu_1(1-\lambda)\int_{C_B} K_{\alpha\delta}(\boldsymbol{x}_0, \boldsymbol{x})\mathscr{V}_\delta^{RBM}(\boldsymbol{x})\,\mathrm{d}l(\boldsymbol{x}) - 8\pi\mu_1(-\Omega_z\sigma_0\delta_{\alpha x} + W(\boldsymbol{x}_0)\delta_{\alpha\sigma} + W(\boldsymbol{x}_0)\delta_{\alpha\varphi}), \tag{3.15}$$

https://doi.org/10.1017/S0022112006004046 Published online by Cambridge University Press

where the point $\boldsymbol{x}_0$ lies on P_1 and $W(x) = V_y + \Omega_z (x - x_c) - u_y^{\infty,1}(x)$,

$$\int_{C_P} \Psi_{\alpha\beta}(\boldsymbol{x}_0, \boldsymbol{x}) \mathscr{F}_\beta(\boldsymbol{x})\, \mathrm{d}l(\boldsymbol{x}) + \int_{C_I} \Psi_{\alpha\beta}(\boldsymbol{x}_0, \boldsymbol{x}) \Delta\mathscr{F}_\beta(\boldsymbol{x})\, \mathrm{d}l(\boldsymbol{x}) - \mu_1(1-\lambda) \int_{C_I} K_{\alpha\delta}(\boldsymbol{x}_0, \boldsymbol{x}) \mathscr{V}_\delta^D(\boldsymbol{x})\, \mathrm{d}l(\boldsymbol{x}) = \mu_1(1-\lambda) \int_{C_B} K_{\alpha\delta}(\boldsymbol{x}_0, \boldsymbol{x}) \mathscr{V}_\delta^{RBM}(\boldsymbol{x})\, \mathrm{d}l(\boldsymbol{x}) - 8\pi\lambda\mu_1(-\Omega_z \sigma_0 \delta_{\alpha x} + W(\boldsymbol{x}_0)\delta_{\alpha\sigma} + W(\boldsymbol{x}_0)\delta_{\alpha\varphi}), \tag{3.16}$$

where the point $\boldsymbol{x}_0$ lies on P_2 and $W(x) = V_y + \Omega_z (x - x_c) - u_y^{\infty,2}(x)$, and

$$\int_{C_P} \Psi_{\alpha\beta}(\boldsymbol{x}_0, \boldsymbol{x}) \mathscr{F}_\beta(\boldsymbol{x})\, \mathrm{d}l(\boldsymbol{x}) + \int_{C_I} \Psi_{\alpha\beta}(\boldsymbol{x}_0, \boldsymbol{x}) \Delta\mathscr{F}_\beta(\boldsymbol{x})\, \mathrm{d}l(\boldsymbol{x}) + 4\pi\mu_1 (1+\lambda)\, \mathscr{V}_\alpha^D(\boldsymbol{x}_0) = 0, \tag{3.17}$$

where the point $\boldsymbol{x}_0$ lies on I. The solution was found using the boundary element method outlined in § 2. Figure 8(*b*) shows a typical particle contour discretization.

3.2. *Results and discussion*

When an axisymmetric particle with top–bottom symmetry translates normal to the axis of revolution in an infinite homogeneous fluid, the shear stress vanishes over the mid-plane. Accordingly, the two-phase flow, generated by the same particle translating parallel to an interface that passes through the particle mid-plane, can be constructed by properly adjusting the viscosities of the fluids in the upper and lower semi-infinite space. When this adjustment is made, the flow field remains unaltered, the interfacial shear stress remains zero, and the normal stress undergoes a discontinuity that is proportional to the difference in the fluid viscosities, requiring high surface tension to restore the flat shape. This construction by superposition emerges from the detailed computations of Ranger (1978) for a circular disk of infinitesimal thickness straddling a flat interface.

In the case of a spherical particle with a hemispherical part in each fluid, $\theta = \pi/2$, we use the well-known solution for Stokes flow due to a translating sphere (e.g. Pozrikidis 1992), and find that the particle traction is given by the simple formula

$$f_x = 0, \qquad f_y = -\frac{3}{2}\frac{\mu_i V_y}{a}, \qquad f_z = 0, \tag{3.18}$$

where $i = 1, 2$, respectively, for the upper and lower fluid. The force and torque exerted on the particle may be easily deduced,

$$F_y = -3\pi\mu_1 V_y a(1+\lambda), \qquad O_z = -\frac{3}{2}\pi\mu V_y a(1-\lambda). \tag{3.19}$$

The expression for the force was derived previously by Ranger (1978) using essentially the same argument. When $\lambda = 1$, we recover Stokes' law for translation in a homogeneous fluid. Construction by superposition for particles with top–bottom symmetry is also possible in the case of rotation about an axis that is normal to the interface, and even when the Navier slip boundary condition is employed. Confirmation is provided by the detailed analysis of O'Neill *et al.* (1986) for a sphere straddling a gas-liquid interface, $\lambda = 0$.

The exact solution for $\theta = \pi/2$ is borne out from our boundary integral computations. Figure 9(*a*) illustrates the distribution of the interfacial traction and velocity coefficients normalized, respectively, by $\mu_1 V_y/a$ and V_y, for $\theta = \pi/2$ and $\lambda = 0$. Note that the normalized velocity coefficients take the value of unity at the particle

https://doi.org/10.1017/S0022112006004046 Published online by Cambridge University Press

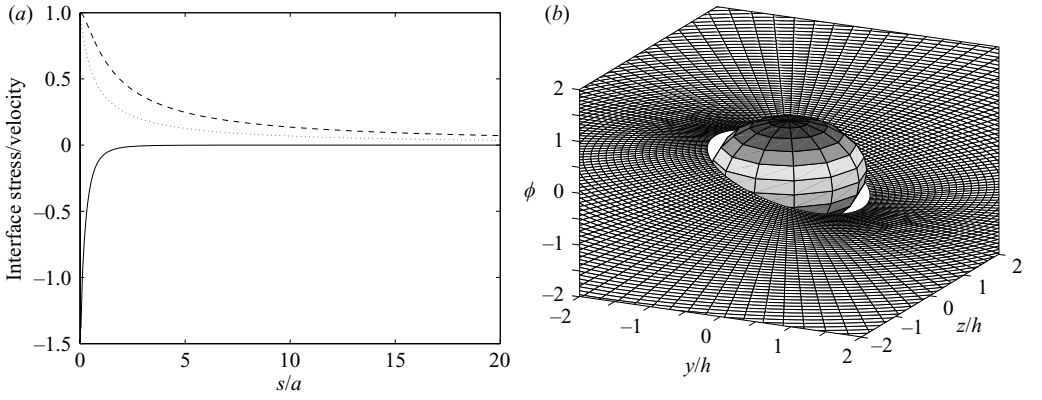


FIGURE 9. Flow due to a translating spherical particle straddling a flat interface for $\theta = \pi/2$ and $\lambda = 0$. (*a*) Distribution of the normalized interfacial traction coefficient $\mathscr{F}_x^D$ (solid line), and velocity coefficients $\mathscr{V}_\sigma^D$ (dashed line), $\mathscr{V}_\varphi^D$ (dotted line), plotted with respect to arclength along the interface. (*b*) Deformed shape of the interface.

θ	$\lambda=0$	0.2	0.4	0.6	0.8	1
$19\pi/20$	−4.34, −2.614	−4.81, −2.13	−5.23, −1.72	−5.62, −1.36	5.97, −1.05	−6.30, −0.767
$3\pi/4$	−4.02, −1.18	−4.50, −1.17	−4.95, −1.12	−5.38, −1.05	−5.79, −0.959	−6.18, −0.854
$\pi/2$	−3.00, −1.50	−3.60, −1.20	−4.20, −0.90	−4.80, −0.600	−5.40, −0.300	−6.00, 0.000
$\pi/4$	−1.49, −1.18	−2.59, −0.528	−3.56, 0.097	−4.45, 0.253	−5.33, 0.565	−6.18, 0.854
$\pi/20$	−0.286, −0.354	−2.08, −0.458	−3.29, −0.285	−4.35, 0.005	−5.34, 0.364	−6.30, 0.767

TABLE 3. Dimensionless force, $\hat{F}_y \equiv F_y/(\pi_1 \mu V_y a)$ (first entry in each cell), and dimensionless torque, $\hat{T}_z \equiv T_z/(\pi\mu_1 V_y a^2)$ (second entry in each cell), exerted on a translating spherical particle straddling an interface, listed as a function of the penetration angle, θ, and viscosity ratio, λ.

surface and drop off algebraically with distance over the interface, as predicted by the exact solution for Stokes flow due to a translating sphere. Figure 9(*b*) illustrates the deformed shape of the interface subject to the zero contact-angle boundary condition at the particle surface. For clarity, the vertical interfacial displacement is displayed on an exaggerated scale as a non-infinitesimal deformation. In this case, the interface bulges downward into the vacuous lower space in front of the translating particle, and upward behind the particle. In other cases, the converse is observed depending on the viscosity ratio and level of particle penetration.

Table 3 shows the dimensionless force and torque exerted on the translating particle for different penetration angles, θ, and viscosity ratios λ in the range [0, 1]. Results for viscosity ratios higher than unity follow by switching the labels of the two fluids. The results for $\theta = \pi/2$ simply repeat the predictions of formulae (3.19). The predictions for $\lambda = 1$ are consistent with the values displayed in figure 4 of Danov *et al.* (2000), though an accurate comparison was prevented by the narrow plotting window of the figure presented by these authors. The data shown in table 3 reveal that the drag force always opposes the particle motion. However, the torque may be positive or negative depending on the fluid viscosities and level of particle penetration. The relation between the force and torque coefficients and the penetration angle or viscosity ratio is not always monotonic.

https://doi.org/10.1017/S0022112006004046 Published online by Cambridge University Press

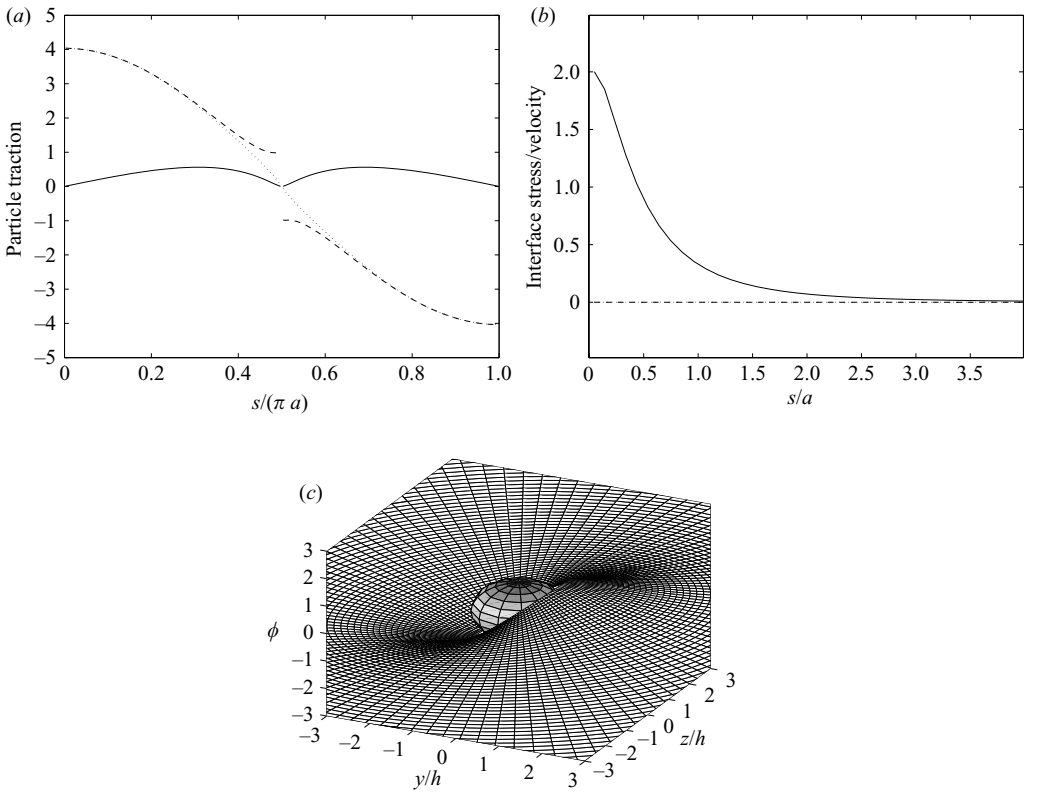


FIGURE 10. Shear flow past a stationary spherical particle straddling an interface for $\theta = \pi/2$ and any value of λ. (*a*) Distribution of the particle traction coefficients $\mathscr{F}_x$ (solid line), $\mathscr{F}_\sigma$ (dashed line), $\mathscr{F}_\varphi$ (dotted line), with respect to arclength measured from the axis of symmetry farthest from the wall. (*b*) Distribution of the normalized interfacial traction coefficient $\Delta\mathscr{F}_x^D$ (solid line), and velocity coefficients $\mathscr{V}_\sigma^D$ (dashed line), $\mathscr{V}_\varphi^D$ (dotted line), plotted with respect to arclength along the interface. (*c*) Deformed shape of the interface subject to the zero contact angle boundary condition. The traction coefficients are normalized by $\mu_1 k_1$, and the velocity coefficients are normalized by $k_1 a$.

Computations were performed for a particle held stationary in simple shear flow parallel to the interface. When each fluid hosts a hemispherical part, $\theta = \pi/2$, the force on the particle is zero, and the torque is given by $T_z = 4.88\pi\mu_1 k_1 a^3$, independent of the viscosity ratio. As a reference, we note that the torque exerted on a sphere held stationary in infinite homogeneous shear flow is $T_z = 4\pi\mu_1 k_1 a^3$. The structure of the flow is illustrated in figure 10.

This remarkable behaviour can be explained by realizing that the upper and lower flows are identical to simple shear flow past a hemispherical protrusion embossed on a plane wall. Indeed, the computed value of the torque is equal to twice that exerted on the protrusion computed analytically by Price (1985) and verified numerically by Pozrikidis (1997*b*). Because the ratio of the shear rates in the upper and lower space is inversely proportional to the viscosity ratio, the shear stress is continuous across the interface after superposition. However, because the sign of the pressure is different on the upper and lower side of the interface, the normal stress undergoes a discontinuity even for fluids of equal viscosity, requiring high surface tension to restore the flat shape.

https://doi.org/10.1017/S0022112006004046 Published online by Cambridge University Press

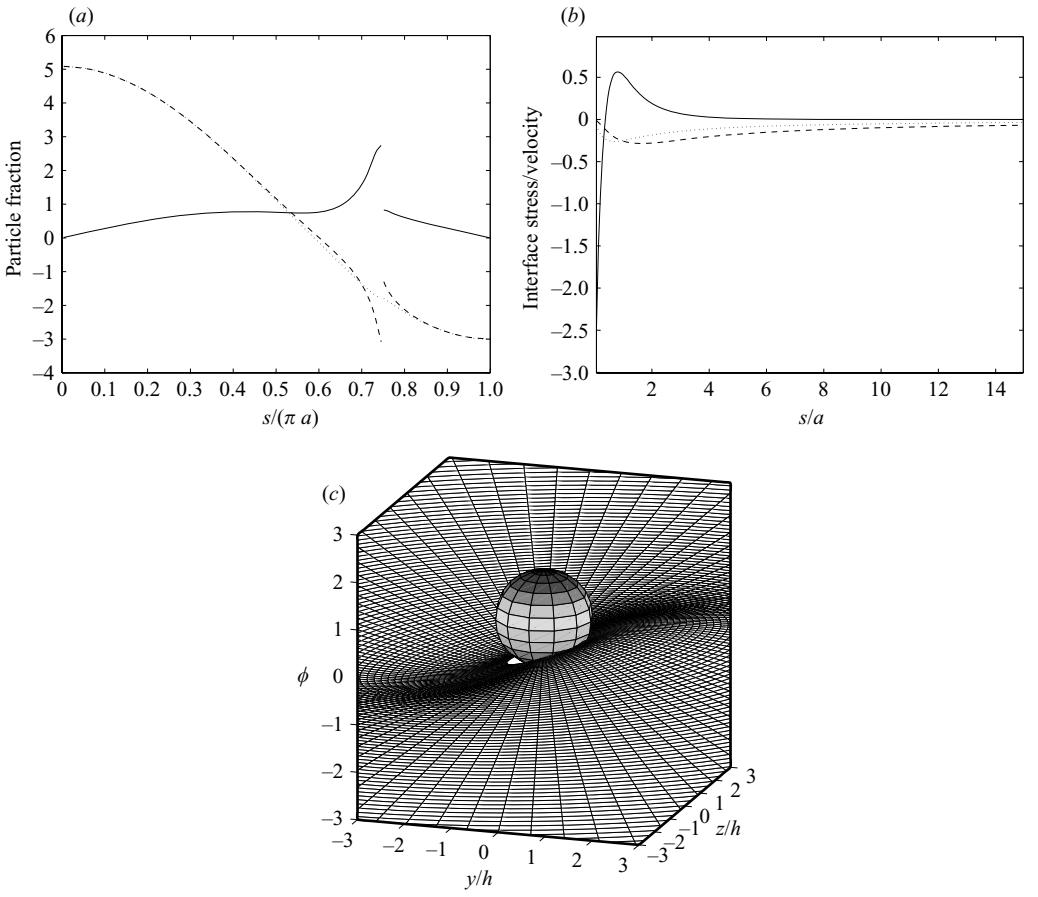


FIGURE 11. The same as figure 10 but for $\theta = \pi/4$ and $\lambda = 1$.

The same behaviour is expected for axisymmetric particles with top–bottom symmetry equally divided by the interface, including the flat disk. However, the vanishing of the force does not imply that a freely suspended particle will rotate without translating under the influence of the simple shear flow, for rotation induces both a force and a torque in the case of unequal fluid viscosities. This simple result for $\theta = \pi/2$ does not extend to different penetration levels. As an example, figure 11 illustrates the structure of the flow for $\theta = \pi/4$ and $\lambda = 1$. In this case, the force and torque exerted on the particle are found to be $F_y = -4.36\pi\mu_1 k_1 a^2$ and $T_z = 4.10\pi\mu_1 k_1 a^3$. Changing the viscosity ratio to $\lambda = 0.1$ yields the significantly different values $F_y = -5.34\pi\mu_1 k_1 a^2$ and $T_z = 5.24\pi\mu_1 k_1 a^3$.

Computations for a rotating sphere where the particle surface velocity has a component normal to the interface around the contact line confirmed the onset of a non-integrable singularity that frustrates the computation of the force, the torque, or both, as discussed by O'Neill *et al.* (1986). Similar difficulties are encountered in the case of a freely suspended particle convected under the influence of a simple shear flow due to the rotary component of the particle motion.

https://doi.org/10.1017/S0022112006004046 Published online by Cambridge University Press

4. Discussion

We have computed the translational and angular velocities of a spherical particle with arbitrary size in simple shear flow parallel to a planar interface, and demonstrated their dependence on the particle distance from the interface and on the viscosity ratio. The results of previous asymptotic analyses for remote particles were found to be surprisingly accurate in the case of translation and rotation, and marginally accurate in the case of free convection, especially for high viscosity ratios. The results of the zeroth-order analysis for a flat interface were used to compute the deformation of the interface to leading order with respect to the capillary number. A projection and a depression were found to develop upstream and downstream from the particle centre under all conditions.

In § 2 of this paper, we considered the force and torque exerted on a spherical particle straddling a planar interface and translating parallel to an interface. Our results confirmed a remarkably simple exact solution uncovered by Ranger (1978) when the particle is immersed halfway in the two fluids. Numerical results were presented for a range of viscosity ratios and particle penetration angles. The drag force exerted on a translating straddling particle is necessary for computing the interfacial diffusivity of small Brownian particles and compact molecules, as discussed by O'Neill *et al.* (1986).

In the case of shear flow past a stationary particle, we have demonstrated that, when the particle is immersed halfway between the two fluids, the flow can be constructed in terms of the semi-infinite flow over a hemispherical protrusion on a plane wall. Consideration of particle rotation around an axis that is parallel to the interface and free convection in simple shear flow was discouraged by the onset of a non-integrable singularity in the traction at the contact line, requiring regularization by means of the slip boundary condition. Luo & Pozrikidis (2006) recently developed an integral formulation that implements the Navier slip boundary condition, and examined the effect of slip on the motion of a sphere near a plane wall. A similar implementation for a particle straddling an interface will be considered in future work.

Straddling marker particles are used to study interfacial rheology in the laboratory. Small particles are desirable in that they prevent significant interfacial deformation, but their motion is hard to observe through an immersed microscope. On the other hand, larger particles cause appreciable deformation due to a meniscus developing around the contact line, and this considerably raises the drag force (Professor K. D. Danov, personal communication). A hydrodynamic analysis taking into account the meniscus will further empower the experimental techniques. The computation of the drag force for a curved interface corresponding to an axisymmetric meniscus will be considered in future research.

The boundary integral method developed in this paper can handle arbitrary particle shapes subject to the condition of rotational symmetry about an axis that is normal to the interface. Examples include prolate and oblate spheroids and flat disks. However, with the exception of the sphere and the zero-thickness disk, the axisymmetry is lost when these particles tumble under the influence of a shear flow. Exceptions occur when oblate particles are positioned at specific heights above the interface, where they translate parallel to the interface without rotation, as has been shown to occur above a plane wall (Pozrikidis 1994*a*). In a different extension, the method can be applied to describe the motion of a spherical particle straddling a spherical interface as implemented on the vesicle experiments of Velikov *et al.* (1997).

https://doi.org/10.1017/S0022112006004046 Published online by Cambridge University Press

The manuscript benefited from insightful comments by Professor K. D. Danov. This research was supported by a grant provided by the National Science Foundation.

REFERENCES

Aderogba, K. 1976 On Stokeslets in a two-fluid space. *J. Engng Maths* **10**, 143–151.

Aderogba, K. & Blake, J. R. 1978*a* Action of a force near the planar interface between semi-infinite immiscible liquids at very low Reynolds numbers. *Bull. Austral. Math. Soc.* **18**, 245–356.

Aderogba, K. & Blake, J. R. 1978*b* Action of a force near the planar interface between semi-infinite immiscible liquids at very low Reynolds numbers: Addendum. *Bull. Austral. Math. Soc.* **19**, 109–318.

Berdan, C. & Leal, L. G. 1982 Motion of a sphere in the presence of a deformable interface: I. Perturbation of the interface from flat: the effects on drag and torque. *J. Colloid Interface Science* **87**, 62–80.

Falade, A. 1986 Hydrodynamic resistance of an arbitrary particle translating and rotating near a fluid interface. *Intl J. Multiphase Flow* **12**, 807–837.

Danov, K. D., Gurkov, T. G., Raszillier, H. & Durst, F. 1998. Stokes flow caused by the motion of a rigid sphere close to a viscous interface. *Chem. Engng Sci.* **53**, 3413–3434.

Danov, K. D., Dimova, R. & Pouligny, B. 2000 Viscous drag of a solid sphere straddling a spherical or flat surface. *Phys. Fluids* **12**, 2711–2722.

Fulford, G. R. & Blake, J. R. 1983 On the motion of a slender body near an interface between two immiscible liquids at very low Reynolds number. *J. Fluid Mech.* **127**, 203–217.

Goldman, A. J., Cox, R. G. & Brenner, H. 1967 Slow viscous motion of a sphere parallel to a plane wall. Part II. Couette flow. *Chem. Engng Sci.* **22**, 653–660.

Lee, S. H., Chadwick, R. S. & Leal, L. G. 1979 Motion of a sphere in the presence of a plane interface. Part 1. An approximate solution by generalization of the method of Lorentz. *J. Fluid Mech.* **93**, 705–726.

Lee, S. H. & Leal, L. G. 1980 Motion of a sphere in the presence of a plane interface. Part 2. An exact solution in bipolar co-ordinates. *J. Fluid Mech.* **98**, 193–224.

Lee, S. H. & Leal, L. G. 1982 The motion of a sphere in the presence of a deformable interface: II. A numerical study of the translation of a sphere normal to an interface. *J. Colloid Interface Sci.* **87**, 62–80.

Luo, H. & Pozrikidis, C. 2006 Effect of slip on the motion of a spherical particle near a wall. Submitted.

Matzen, G. W. 1997 Effect of microscale protrusions in local fluid flow and mass transport in the presence of forced convection. Doctoral Dissertation in Chemical Engineering, UC, Berkeley, 1997.

O'Neill, M. E. & Ranger, K. B. 1979 On the rotation of a rotlet or sphere in the presence of an interface. *Intl J. Multiphase Flow* **5**, 143–148.

O'Neill, M. E., Ranger, K. B. & Brenner, H. 1986 Slip at the surface of a translating-rotating sphere bisected by a free surface bounding a semi-infinite viscous fluid: removal of the contact-line singularity. *Phys. Fluids* **29**, 913–924.

Pozrikidis, C. 1992 *Boundary Integral and Singularity Methods for Linearized Viscous Flow*. Cambridge University Press.

Pozrikidis, C. 1994*a* The motion of particles in the Hele-Shaw cell. *J. Fluid Mech.* **261**, 199–222.

Pozrikidis, C. 1994*b* Shear flow over a plane wall with an axisymmetric cavity or a circular orifice of finite thickness. *Phys. Fluids* **6**, 68–79.

Pozrikidis, C. 1997*a* *Introduction to Theoretical and Computational Fluid Dynamics*. Oxford University Press.

Pozrikidis, C. 1997*b* Shear flow over a protuberance on a plane wall. *J. Engng Maths* **31**, 31–44.

Pozrikidis, C. 2000 Effect of pressure gradient on viscous shear flow over an axisymmetric depression or protuberance on a plane wall. *Computers Fluids* **29**, 617–637.

Pozrikidis, C. 2006 Motion of a spherical particle in film flow. *J. Fluid Mech.* **566**, 465–475.

Price, T. C. 1985 Slow linear shear flow past a hemispherical bump in a plane wall. *Q. J. Mech. Appl. Maths* **38**, 93–104.

https://doi.org/10.1017/S0022112006004046 Published online by Cambridge University Press

Ranger, K. B. 1978 The circular disk straddling the interface of a two-phase flow. *Intl J. Multiphase Flow* **4**, 263–277.

Shatz, L. 2004 Indirect boundary element method for unsteady linearized flow over prolate and oblate spheroids and hemispheroidal protuberances. *Intl J. Numer. Meth. Fluids* **44**, 147–174.

Stoos, J. A. & Leal, L. G. 1989 Particle motion in axisymmetric stagnation flow toward an interface. *AIChE J.* **35**, 196–212.

Stoos, J. A. & Leal, L. G. 1990 A spherical particle straddling a fluid gas interface in an axisymmetric straining flow. *J. Fluid Mech.* **217**, 263–298.

Velikov, K., Dietrich, C., Hadjiisky, A., Danov, K. D. & Pouligny, B. 1997 Motion of a massive microsphere bound to a spherical vesicle. *Europhys. Lett.* **40**, 405–410.

Yang, S.-M. & Leal, L. G. 1983 Particle motion in Stokes flow near a plane fluid–fluid interface. Part 1. Slender body in a quiescent fluid. *J. Fluid Mech.* **136**, 393–421.

Yang, S.-M. & Leal, L. G. 1984 Particle motion in Stokes flow near a plane fluid–fluid interface. Part 2. Linear shear and axisymmetric straining flows. *J. Fluid Mech.* **149**, 275–304.

Yang, S.-M. & Leal, L. G. 1989 Motions of a porous particle in Stokes-flow near a plane–fluid interface. *Physicochemical Hydrodynamics* **11**, 543–569.

Yang, S.-M. & Leal, L. G. 1990 Motions of a fluid drop near a deformable interface. *Intl J. Multiphase Flow* **16**, 597–616.

Yiantsios, S. G. & Davis, R. H. 1990 On the buoyancy-driven motion of a drop towards a rigid surface or a deformable interface. *J. Fluid Mech.* **217**, 547–573.

https://doi.org/10.1017/S0022112006004046 Published online by Cambridge University Press